J. Fluid Mech. (1996), *vol.* 310, *pp.* 1–37

The effects of excitation on the coherent and random motion in a plane wall jet

By M. D. ZHOU, C. HEINE AND I. WYGNANSKI†
Department of Aerospace Engineering, The University of Arizona, AZ 85721, USA

(Received 14 October 1994 and in revised form 14 August 1995)

Three components of velocity fluctuations were measured in a plane turbulent wall jet which was modulated periodically by a sinusoidal pressure fluctuation in its settling chamber. The experiment was carried out in a closed-loop wind tunnel in the absence of an external stream at Reynolds number $Re_j = U_j b/\nu = 6900$ and Strouhal number $St_j = fb/U_j = 9.5 \times 10^{-3}$, where b is the width of the slot from which the jet emerges at an efflux velocity U_j. A detailed comparison is provided with similar measurements made in a natural, unexcited turbulent wall jet. One of the purposes of this experiment was to establish the kinetic energy transfers which take place in the wall jet under controlled perturbations. More specifically, we were interested in determining the interactions occurring between the steady mean flow, the coherent eddies and the 'random' turbulent fluctuations. We used the triple decomposition of the equations of motion as suggested by Hussain (1983) and quickly observed that the usefulness of this decomposition depends on the definition of coherent motion, which is ambiguous in the presence of phase jitter. Two such definitions were considered and the results are discussed in the experimental case-study provided. An attempt is made to define quantitatively the intensities of the coherent motion in externally excited, wall-bounded flows. It is a case-study and not a parametric investigation aimed at maximizing the effects of period oscillations on the wall jet.

1. Introduction

Some effects of periodic two-dimensional excitation on the structure of the wall jet were investigated by Katz, Horev & Wygnanski (1992, hereinafter referred to as KHW) who discovered that the most important practical consequence of modulating of the flow is the appreciable reduction in skin friction. The reasons for this effect are largely unknown; however, since the two-dimensional modulation also enhanced the spanwise coherence of the large eddies the two observations were linked together. It was anticipated that the spanwise order introduced by the external excitation would also reduce the intensity of the spanwise velocity fluctuations as it did in the plane mixing layer (Oster & Wygnanski 1982). We have thus embarked on measuring the effects of external excitation on all three components of the velocity fluctuations in the wall jet.

Only a handful of experimenters (e.g. Irwin 1973; Guitton & Newman 1977; Alcaraz 1977) have measured more than the streamwise component of the velocity fluctuations and there is considerable disagreement among them (see Launder & Rodi 1981). Some of the disagreement stems from attempts to scale the turbulent intensities with the maximum mean velocity in the jet because these two quantities decay at a different rate in the direction of streaming. The use of the nozzle dimension as an important lengthscale of the experiment may have also contributed to the scatter. Both

† Also Lazarus Professor of Aerodynamics–Tel Aviv University.

assumptions were shown to be of questionable validity (Wygnanski, Katz & Horev 1992; Zhou & Wygnanski 1993, hereinafter referred to as ZW) and it was therefore decided to measure as many quantities as necessary to construct the turbulent kinetic energy balance in the forced and in the natural, turbulent wall jets.

The kinetic-energy balance in a modulated flow enables one to assess in principle the interaction occurring between the coherent (modulated) motion and the incoherent turbulence. Such an interaction was always neglected in the past because it was considered unimportant in free turbulent shear flows and because it is difficult to measure. Hussain (1983) decomposed the velocity and pressure into steady, coherent, random components and considered theoretically the energy fluxes among them. Energy is extracted from the mean flow to feed directly the coherent and random fluctuations through the production terms appearing in the equations, but some of the random fluctuations might have extracted energy from the coherent motion as well. Thus the assessment of the energy flux between the coherent and the random fields is important to know. It is generally assumed that more energy is extracted from the coherent eddies by the random ones than vice versa, because this assumption fits the energy cascade concept even though it was not proven experimentally. It was also argued that most of the viscous dissipation is associated with the small-scale random motion (Hussein 1983), because the small random eddies are contained in the large coherent ones like pebbles inside a moving pot. Most of the friction occurs among the pebbles but some friction may occur between the pebbles and the walls of the pot as well. Although there might be nothing wrong with these concepts, they should be verified experimentally, particularly when one identifies the large coherent motion with the predominant instabilities of the flow. Since the flow perturbations resulting from instability of the boundary layer decay owing to the presence of viscosity and viscosity causes dissipation in turbulent boundary layers, one may not dismiss the possibility that direct dissipation might reduce the energy of the large eddies as well. It was also noted (Zhou, Heine & Wygnanski 1993) that the turbulent wall jet contains two types of large coherent structures: one associated with the wall boundary layer and the other with the exterior, jet-like region. Although these structures differ appreciably in size and in their predominant location in the flow, they could propagate at similar velocities and exchange energy between them. Consequently the exchange of energy between the mean flow and the different types of eddies, or among the coherent eddies themselves, or between the coherent and the random eddies should be known if one is to control the flow in any manner.

The present experiment endeavours to determine the energy transfers that take place in a wall jet. External excitation in this case is used primarily as a diagnostic tool rather than a tool for control or modification of the flow. It helps one to define quantitatively the velocity perturbations associated with coherent structures. Although such definition is not unique, it represents a major advance over a qualitative description. For this reason the frequency selected for excitation corresponds to the predominant frequency observed naturally in the wall region approximately 100 slot widths downstream of the nozzle at the selected flow conditions. The experiment was carried out in the facility described by ZW at Reynolds number based on the jet velocity and slot width of 6900. The efflux velocity of the jet was $32\ \mathrm{m\ s^{-1}}$ which was at times modulated at an amplitude of 5% at a Strouhal number based on the excitation frequency and nozzle dimension of 9.5×10^{-3}. The measurements were carried out with hot-wire anemometers and hot-wire probes arranged in X and V arrays built specially for measuring transverse and lateral fluctuations in the flow. More details about the experimental facility can be found in earlier papers (e.g. ZW and Heine 1994).

2. Discussion of results

2.1. *Mean flow measurements*

The mean velocity profiles were measured with a single hot-wire probe at a variety of streamwise locations ranging from 30 to 200 slot widths downstream of the nozzle. In this region the mean flow is self-similar, as observed earlier by many investigators (e.g. Tailland & Mathieu 1967, or Karlsson, Ericsson & Persson 1992). Since the measurements were made in a closed-loop wind tunnel, the surrounding fluid was not entirely quiescent (i.e. there was a small but finite velocity in the free stream) because the jet acted as an ejector and moved the fluid in this large, recirculating volume of air. Although the free-stream velocity induced by the wall jet was only 8 % of the maximum velocity measured in the area of interest, it had to be accounted for. For this reason the data were normalized in a manner suggested by ZW for strong wall jets in streaming flow (for which $U_\infty/U_m < 0.5$), and the results are illustrated in figure 1. The insert shown in this figure represents schematically the two lengthscales and two velocity scales used in collapsing the data onto a dimensionless self-similar curve. Figure 1 represents therefore a plot of

$$\frac{U}{U_m} \quad \text{versus} \quad \frac{y-y_m}{y_m} \quad \text{when} \quad y \leqslant y_m,$$

$$\frac{U-U_\infty}{U_0} \quad \text{versus} \quad \frac{y-y_m}{y_0} \quad \text{when} \quad y > y_m,$$

where $U_0 = U_m - U_\infty$ and $y_0 = y_2 - y_m$.

The ratio of the two lengthscales y_m and y_0 is constant whenever the ratio between the free-stream velocity and the jet efflux velocity is not changed and therefore, a single lengthscale would have sufficed to represent the current data. The numerical value of $y_m/y_2 \approx 0.2$ indicates that U_∞/U_j is small (see figure 1 and ZW, figure 3). The physical form of the mean velocity profile was not distorted, in this and all other figures representing the normalized distance from the surface, in spite of the use of two different lengthscales to normalize the data. This was achieved by compressing the physical scale of the inner region by the ratio corresponding to y_m/y_2. The solid line represents the best fit to the velocity profiles measured in the absence of external perturbations. Thus the distortion of the mean velocity profile by the imposed oscillations is minor almost everywhere in the flow.

The rate of spread of the outer lengthscale of the jet (y_0/b) with and without external excitation is plotted in figure 2(*a*). Although the difference in the rate of spread between the two sets of data is small and indistinguishable for $x/b < 100$ it affects the loss of mean kinetic energy to the coherent motion. The rate of spread of the inner lengthscale y_m/b is not affected by the external excitation in the range of distances considered (figure 2*a*). Even a relatively weak external excitation (see KHW) distorts the velocity profile near the solid surface in a manner which reduces the mean vorticity of the fluid in this region and with it the loss of momentum due to friction with the surface. It was reasoned that periodic, plane excitation of the outer flow enhances the large eddies prevailing in the outer layer of the wall jet and enables them to transport low-momentum fluid towards the surface. In this case the wall jet was forced at $St_j = 9.5 \times 10^{-3}$ at an approximate level corresponding to 5 % of the jet efflux velocity. The forcing level is defined here as the ratio between the time-averaged r.m.s. velocity and the mean velocity measured near the centre of the nozzle exit. This quantity includes the turbulence (random fluctuation) level at the exit. A more precise definition of the

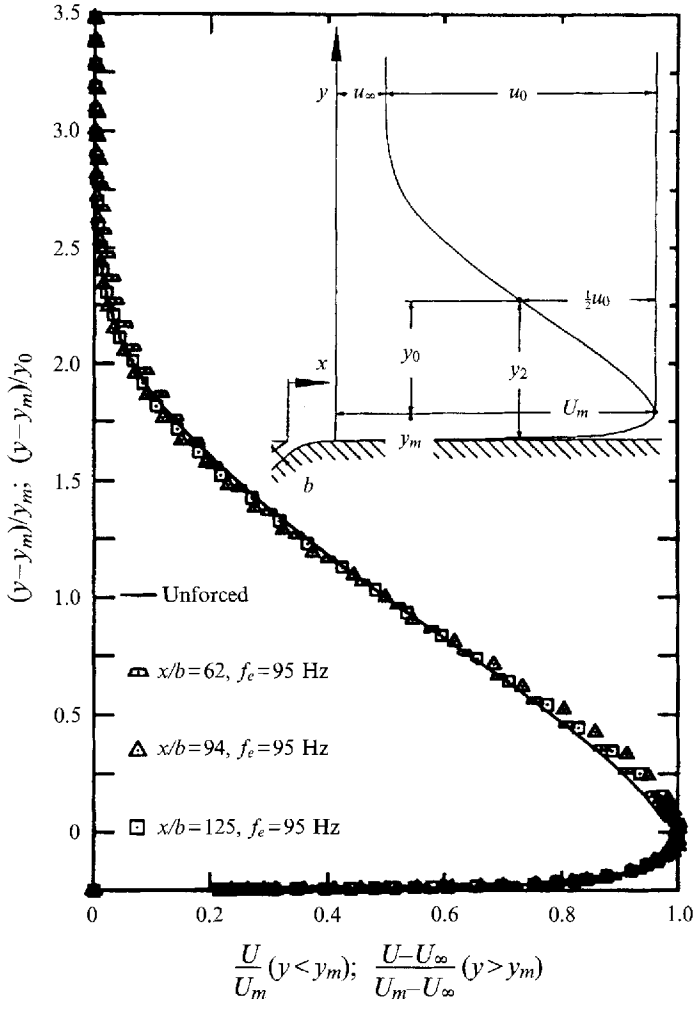

FIGURE 1. The influence of forcing on the mean velocity profile.

forcing amplitude would have contained only the r.m.s. value of the phase-averaged fluctuations attributed to the excitation. In reality therefore, the jet is forced at a lower amplitude than the 5% specified. A simple subtraction of the turbulence level at the nozzle (which is of the order of 0.7%) is not necessarily correct because the spectrum of the turbulence at the nozzle exit contains peaks at numerous preferred frequencies. The relative skin friction reduction due to the excitation at the specified St_j and amplitude is plotted in figure 2(*b*) against distance from the nozzle. The maximum local skin friction reduction is 7% and occurs around $x/b = 150$.

The skin friction was calculated from the slope of the mean velocity in the viscous sublayer; this slope was constant as long as it was based on the data acquired below the y-location corresponding to $U/U_m = 0.37$ or below $y^+ = 7$. The repeatability of the data was good whenever the measurements were carried out with and without the presence of the excitation consecutively at a given streamwise location. The loudspeaker used to force the flow was simply switched 'on' and 'off' before moving the probe to another x-location. The velocities measured in the viscous sublayer were also used to determine the distance of the probe from the wall. These distances were calculated

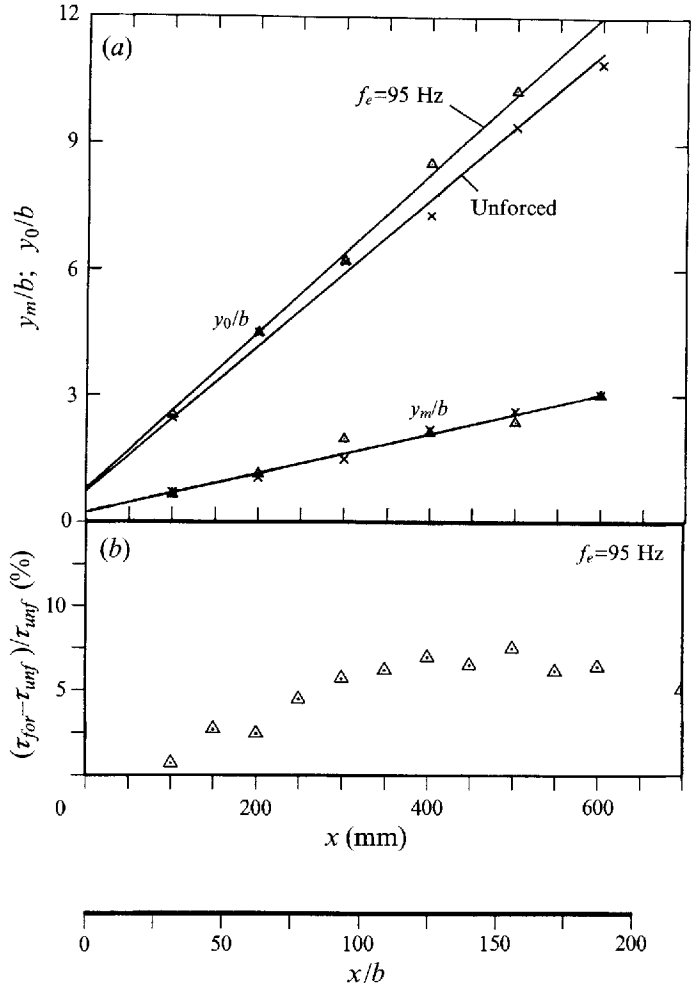

FIGURE 2. The influence of forcing on (*a*) the spreading of wall jet and (*b*) the skin friction reduction.

independently with and without external forcing and the two results differed usually by less than 2 μm.

The mean flow parameters scale with the excess momentum flux near the nozzle exit,

$$J \equiv \int_0^\infty U(U-U_\infty)\,\mathrm{d}y \approx U_j(U_j-U_\infty)b,$$

and the viscosity ν. The former quantity degenerates to the jet momentum in the total absence of an external stream. Both J and ν are combined with x to yield a dimensionless streamwise distance ξ:

$$\xi = xJ/\nu^2.$$

This scaling was suggested first by Narasimha, Narayan & Parthasarathy (1973) in the absence of an external stream and was extended recently by ZW to include the effects of a relatively weak external stream whose velocity did not attain 50% of the maximum velocity in the jet. The results for the mean lengthscale and velocity scale as well as for the wall stress agree with the correlations suggested by ZW and therefore

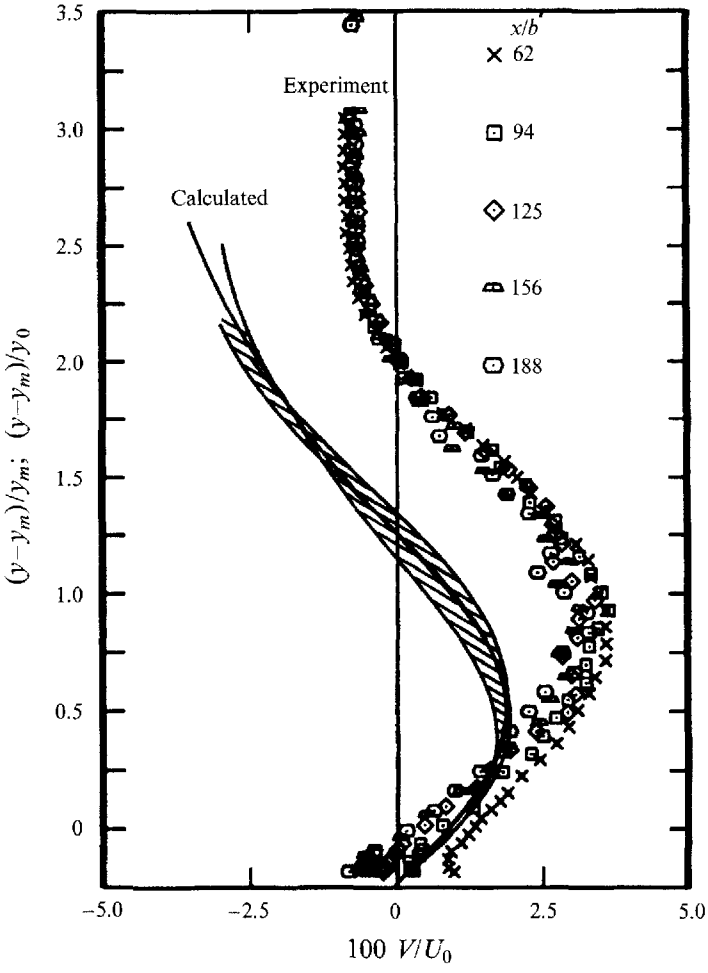

FIGURE 3. The normal mean velocity component.

will not be repotted here. These can be simply determined by the following relationships

$$\frac{y_2 J}{R\nu^2} = 1.857\xi^{0.87};\quad \frac{y_m J}{\nu^2} = 0.27\xi^{0.87};\quad \frac{y_0 J}{R\nu^2} = 0.61\xi^{0.91};$$

$$\frac{\tau_w R\nu^2}{\rho J^2} = 0.0057\xi^{-0.92};\quad \frac{U_m \nu R}{J} = 0.68\xi^{-0.43};\quad \frac{U_0 \nu}{J} = 0.86\xi^{-0.44},$$

where $R = (U_j - U_\infty)/(U_j + U_\infty)$.

The normal mean velocity component V was actually measured using an X-wire and the data were compared with results calculated from local U-distributions by using continuity (figure 3). The shaded area corresponds to the maximum scatter in these calculations. Since $V_m/U_m < 3\%$ at all x-locations, while the calibration of the individual wires in an X-array is only accurate to within 1%, it is not surprising that the agreement between the calculated V and the measured one is not good; it is, however, within the expected error range of the hot wires. The data are presented because they give an estimate for the mean-flow angle $\alpha = \arctan(V/U)$ at the outer part of the wall jet and demonstrate that the boundary-layer approximation is appropriate in the analysis of this flow. Since $(\alpha)_{y\to\infty} < 12°$ (based on estimates made

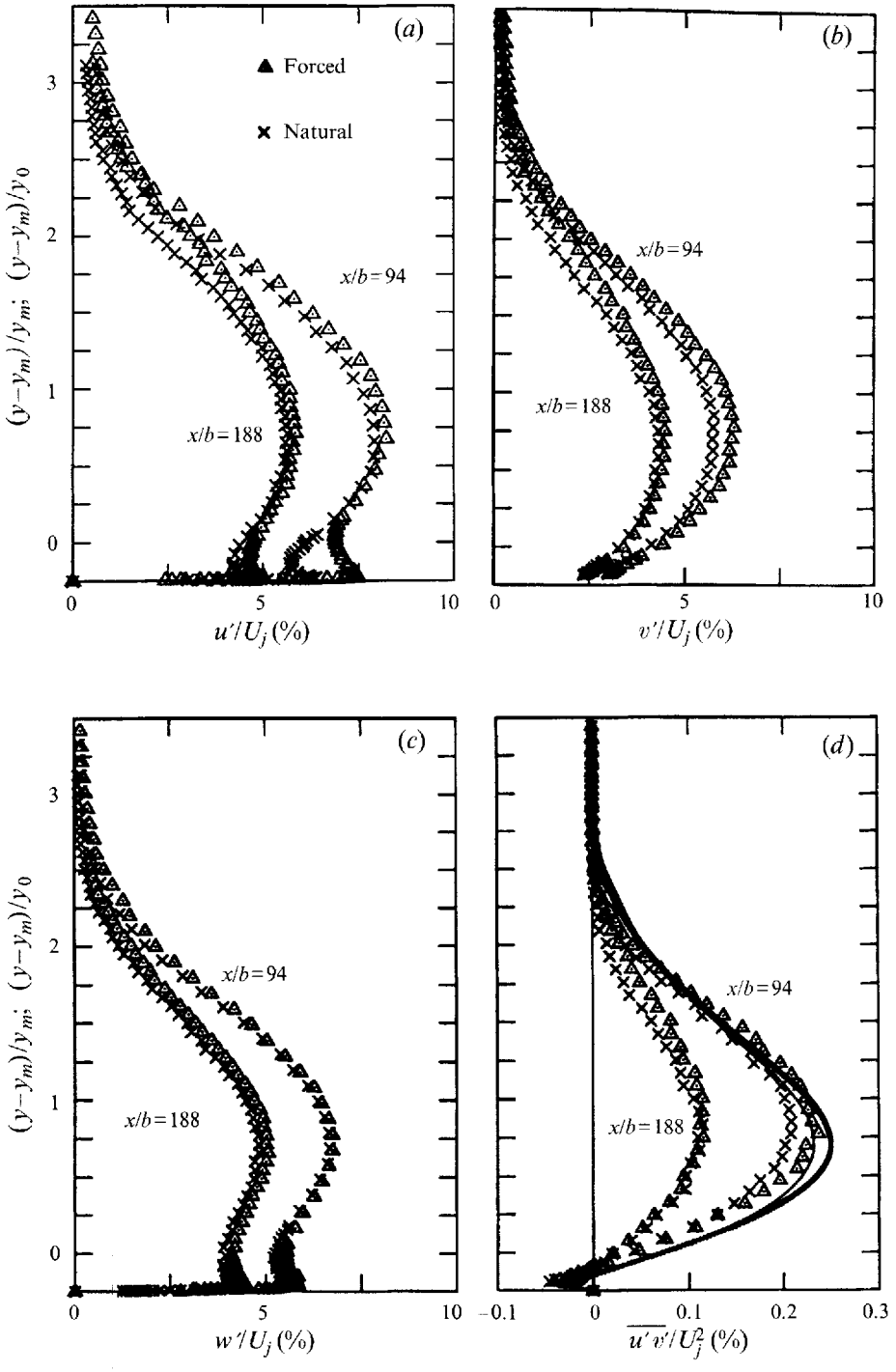

FIGURE 4. The influence of forcing on the turbulence intensity and Reynolds stress.

using the continuity equation and $(\alpha)_{y\to\infty} < 4°$ if one were to assume that the X-wire measurements are valid) the advantages of investigating the wall jet in a closed wind-tunnel facility become obvious because experiments carried out in 'still surroundings' yield $(\alpha)_{y\to\infty} = 90°$.

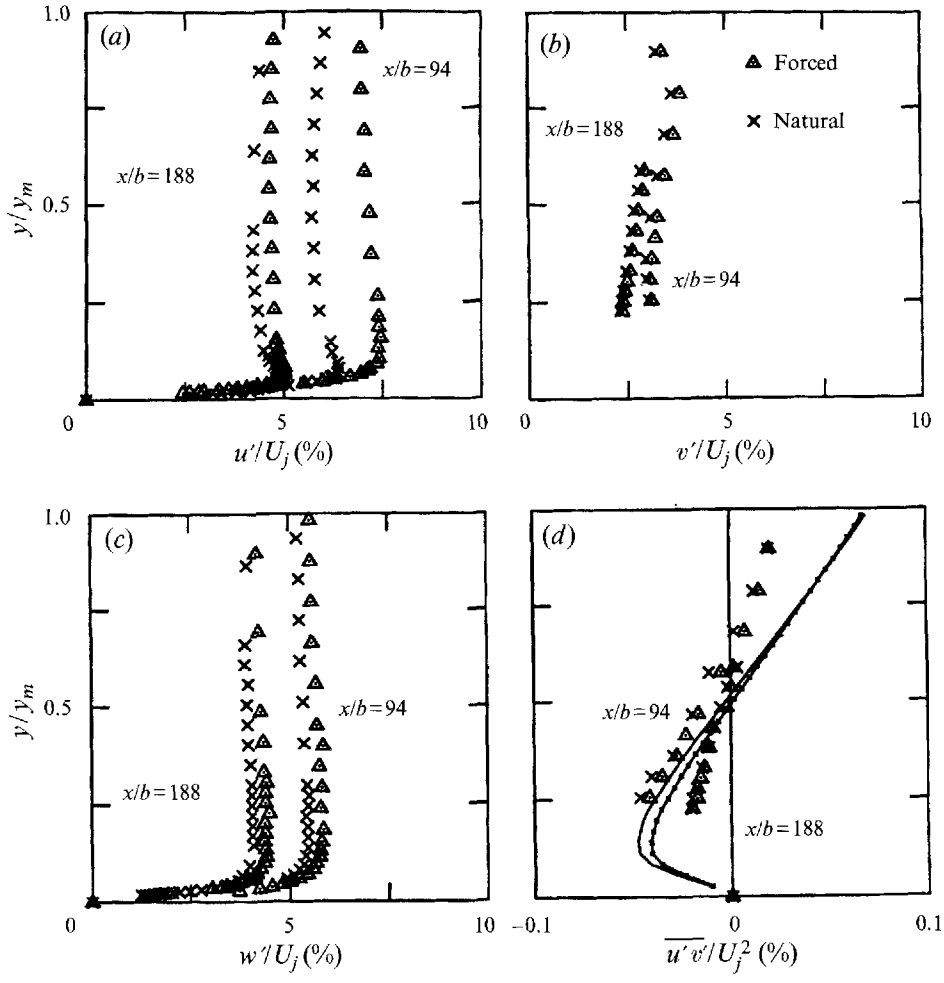

FIGURE 5. The influence of forcing on the turbulence intensity and Reynolds stress near the surface.

2.2. *Velocity fluctuations (conventional Reynolds-averaged quantities)*

The lateral distribution of the fluctuating intensities of the three components of velocity and of the Reynolds stress measured at $x/b = 94$ and 188 are plotted in figures 4 and 5. Two sets of data for each quantity are presented: one for the natural (unperturbed) wall jet (marked by $\times$ symbols) and the other for the externally excited flow at $St_j = 9.5 \times 10^{-3}$ (marked by $\triangle$). The comparison is made at two streamwise locations only, in order to bring out the effects of excitation on those quantities. The values are normalized by the jet exit velocity U_j which was maintained at a constant level throughout the experiment and by the local lengthscales measured in the absence of excitation. This was done in order to assess the effect of excitation on the level of the fluctuations and their distribution in the most clear manner.

The utility of multi-wire probes in measuring the velocity fluctuations correctly near the surface is rather limited when the inner lengthscale y_m is small and becomes comparable with a typical dimension of the probe. The r.m.s. of the u'-component of the velocity fluctuations (i.e. $(\overline{u'^2})^{1/2}$ which will often be simply referred to as u' etc.), automatically measured by X-write or V-wire probes, was therefore compared with the

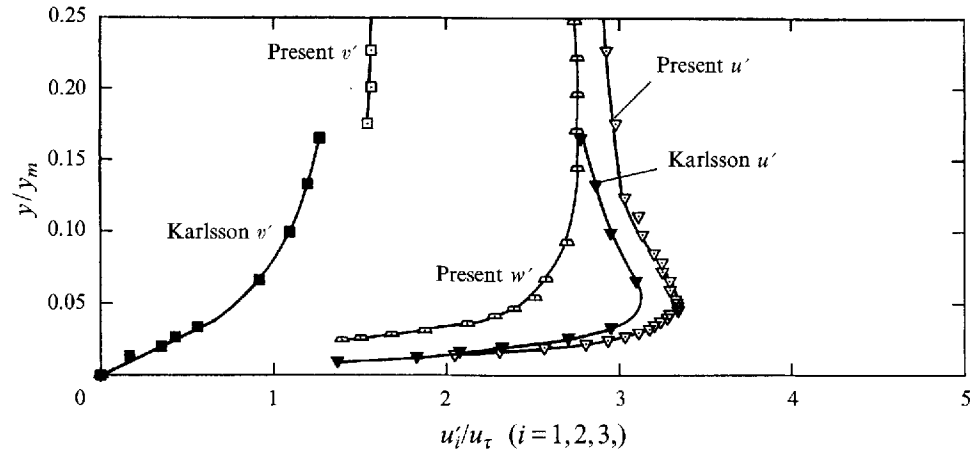

FIGURE 6. Comparison between the present data and Karlsson *et al.*'s (1992).

output of the single wire which did not suffer from the spatial resolution problem. The deviations from the u' measured by a single wire were insignificant far away from the surface but became acute near the wall. The maximum deviations in the results presented are estimated to be 9% at $x/b = 94$ and 6% at $x/b = 188$ very close to the wall; these numbers should be born in mind when consistency checks and comparisons to other investigator's data are being made.

The lateral distributions of the r.m.s. of the u' and w' components (figure 4*a*, *c*) have two peaks: one in the outer part of the flow, around $(y-y_m)/y_0 = 0.8$ and one very near to the wall. The r.m.s. distribution of v' possesses only one peak in the outer region. No data could be acquired closer to the surface than shown in figure 5(*b*) but the slope $(\partial v'/\partial y) > 0$ even at $y/y_m = 0.25$. Furthermore, in all boundary-layer and pipe-flow experiments (Klebanoff 1955; Laufer 1954) the inhibiting effect of the solid surface on the v' fluctuations extended further away than for the other velocity components. Rotta (1962) reasoned, by using the no-slip conditions and the continuity equation, that not only $v'_{wall} = 0$ but also $(\partial v'/\partial y)_{wall} = 0$ and therefore the influence of the surface is more pronounced on v' than on the other components. Karlsson *et al.* (1992) used an LDA to measure the two components of the velocity fluctuations in water at a comparable Reynolds number. They were able to acquire data much closer to the surface (the closest point reported by Karlsson *et al.* was at $y^+ = 3$) without suffering from the problems encountered with hot-wire arrays. They also did not observe a peak in the intensity of the v'-fluctuations in the inner part of the wall jet. Karlsson's *et al.*'s measurements agree fairly well with thc present data in the region in which there is an overlap (figure 6): their u' measurements are in good agreement with ours near the surface with maximum deviation of 5% at $y/y_m > 0.03$ while their v' data tend to our results at $y/y_m > 0.15$.

It was observed that the w' component is larger than the v' one at all $(y-y_m)/y_0 < 2$. This aspect had to be checked, since these two components were measured with different probes. The X-wire probe was therefore rotated by 90° and the results were shown to be consistent. A careful comparison with previous wall-jet investigations revealed that this observation is universal. The data of H. Abrahamsson, B. Johansson & L. Loefdahl (1994, personal communication) gave $(v'/w')_{max} = 0.84$, while the results of Irwin (1973) for the self-preserving wall jet in a specially tailored pressure gradient yielded $(v'/w')_{max} = 0.88$. These numbers compare well with the present

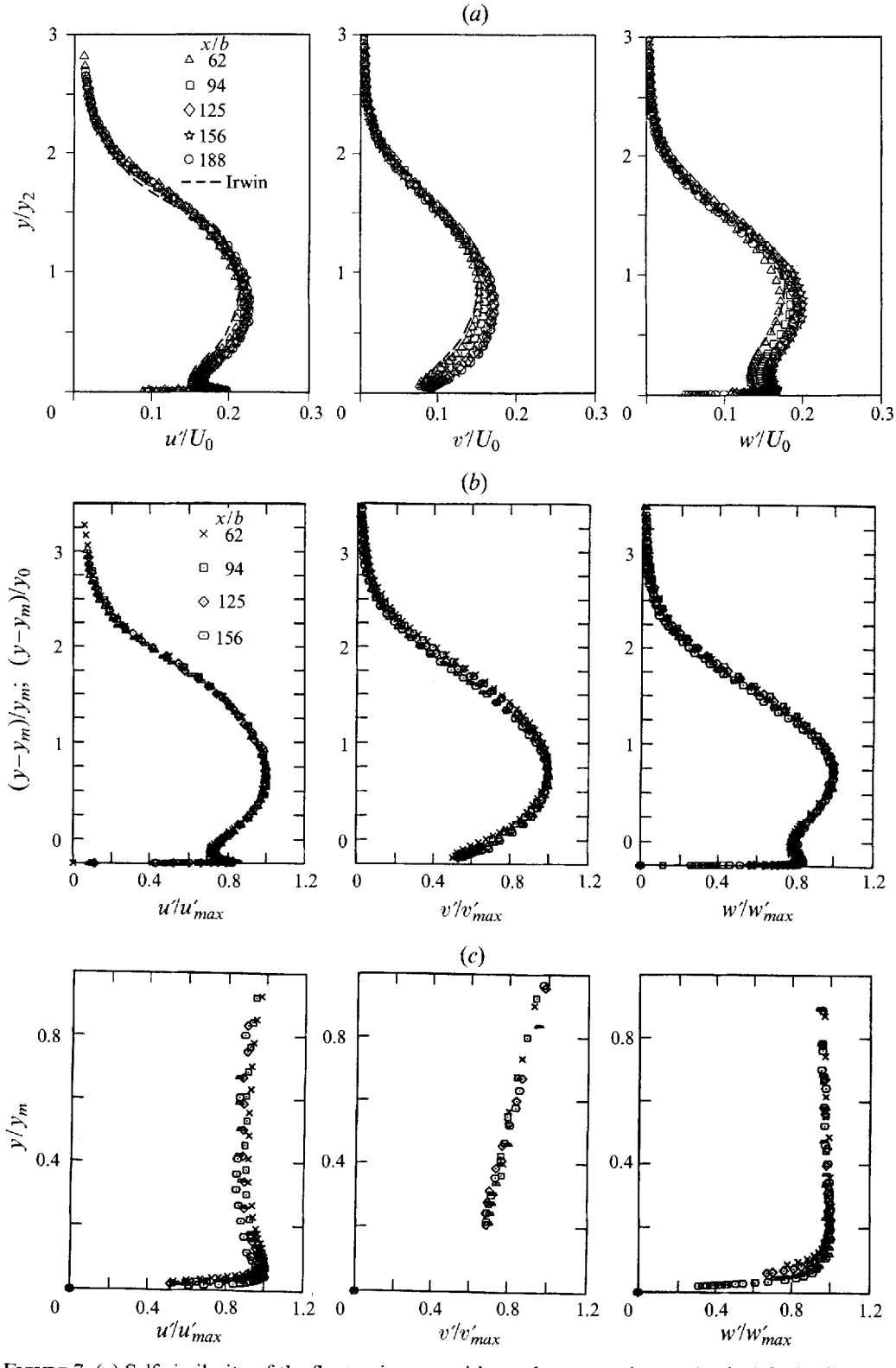

FIGURE 7. (*a*) Self-similarity of the fluctuating quantities and a comparison to Irwin (1973). (*b*) Data normalized by outer-region local maxima. (*c*) Data normalized by inner-region local maxima.

observations for which $(v'/w')_{max} = 0.87$. The lateral distribution of all three components of the velocity fluctuations are compared with Irwin's data (figure 7*a*) because he also made a detailed energy budget for his wall-jet flow. The agreement is surprisingly good in spite of the following disparities in the experimental conditions. (i) Irwin's experiments were carried out in an adverse pressure gradient in which the ratio between the free-stream and the maximum velocity in the jet was constant everywhere ($U_1/U_m = 0.38$), while in our experiment $U_\infty/U_m = 0.08$ near the nozzle and increased slightly with increasing x. The variation of U_m with x is not sensitive to pressure gradient in this range of velocity ratios since Irwin observed that $U_m \propto x^{-0.428}$ and Wygnanski *et al.* (1992) observed $U_m \propto x^{-0.448}$ in the absence of an external stream. (ii) Irwin's Reynolds number Re_j was approximately four times larger.

The deviations from self-similarity relative to the mean velocity scale (figure 7*a*) could have been attributed to the variations in U_∞/U_m if we had not observed a similar lack of self-similarity when $U_\infty/U_m = 0$ (Wygnanski *et al.* 1992, figure 6). Irwin (1973, figure 12) also did not observe good self-similarity in his turbulent intensity distributions in spite of the large Re_j of his experiment. Abrahamsson *et al.* (personal communication) indicates that a self-similar turbulent intensity is possible in a limited range of streamwise distances ($70 < x/b < 150$) but their own data taken further downstream refute this assertion. The lack of self-similarity suggests an absence of equilibrium between the mean flow and the turbulence over the range of distances considered ($62 < x/b < 188$ considered here).

When each component of the velocity fluctuations is normalized by its own maximum and the data for u' and w' are normalized by their respective local maxima (one for the outer region (figure 7*b*) and the other for the inner region of the flow (figure 7*c*)) self-similarity is restored. This suggests that not only does the mean velocity have two scales (an outer scale $(U_m - U_\infty)$ and an inner scale U_m) whenever the outer flow is not quiescent but so does the turbulent intensity. The turbulence in the inner and outer regions of the wall jet might have been generated locally wherever a large concentration of mean vorticity exists; the resultant intensities however, may depend on the interaction among the larger eddies originating at different regions of the flow.

The lateral distributions of the Reynolds stress are plotted on figure 4(*d*) and compared at $x/b = 94$ with the stress calculated from the mean equation of motion (the two solid curves plotted on that figure, one for the natural jet and one for the forced flow). The normal stress term: $(\partial/\partial x)(\overline{u'^2} - \overline{v'^2})$ appearing in the mean equation of motion was neglected in this calculation. Experimental data justifies this omission with the exception of the location at which $\overline{u'v'} \to 0$ (i.e. at $0.6 < y/y_m < 1$), and this case will be discussed later in detail. The comparison between the measured stress and the calculated one is excellent in the outer region of the flow but it deteriorates somewhat closer to the surface. The maximum calculated stress overestimates the measured one by 10% in the natural flow and by 5% in the externally excited flow. Some of the discrepancy might be attributed to the spatial resolution of the x-wire probe; nevertheless the agreement is good enough to suggest that the flow is two-dimensional in the mean.

The location at which the maximum Reynolds stress was observed appears to be sensitive to the details of the experiment: Abrahamsson *et al.* (personal communication) located the maximum at $(y - y_m)/y_0 = 0.55$, Karlsson *et al.* at 0.7, Irwin close to 0.75, and the present results at 0.8. It is quite possible that the presence of an external stream or pressure gradient influences this location. One should also recall that the Reynolds stress (i.e. the time-averaged $u'v'$ product, $\overline{u'v'}$) does not vanish at y_m.

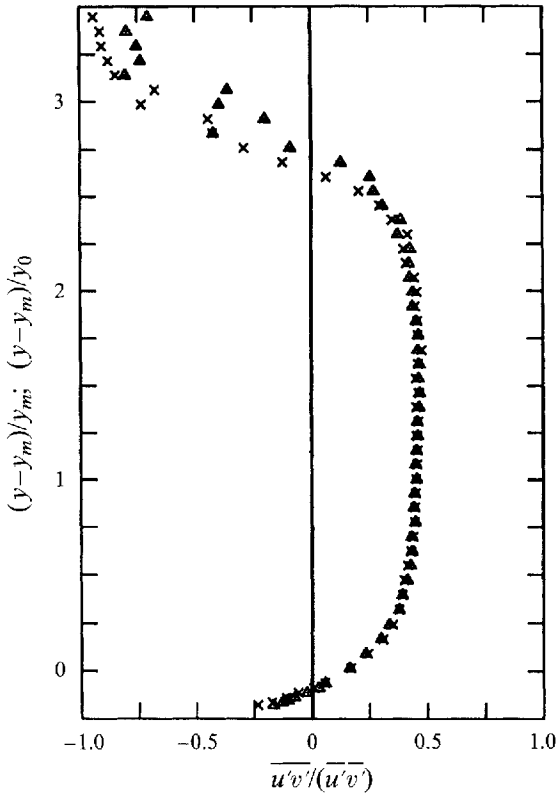

FIGURE 8. The influence of forcing on the ratio between the Reynolds stress and the turbulence intensity.

This is an indication that the mean motion is not in equilibrium with the energy-containing turbulent eddies at every location in the flow field. This effect was first reported by Kruka & Eskinazi (1964) and it points out the shortcomings of many simple turbulence models. Surprisingly, the maximum Reynolds stress correlation $(\overline{u'v'}/(\overline{u'^2})^{1/2}(\overline{v'^2})^{1/2})_{max}$ measured here, and by all the above-mentioned investigators, was approximately 0.49. The value of this correlation was substantially constant across the outer region of the jet (i.e. for $0.3 < (y-y_m)/y_0 < 2.3$) and it was not affected by the external excitation (figure 8). This correlation is also approximately 20% higher than the one observed in a turbulent boundary layer, suggesting a more efficient momentum transport across the outer part of the wall jet than across a boundary layer. In the boundary-layer case, this correlation is constant outside the viscous sublayer while in the wall jet it is only constant in the outer flow (i.e. where $y > y_m$).

The effect of the chosen external excitation on the three fluctuating components of velocity and on the Reynolds stress in the outer part of the wall jet is minor. The maximum v' fluctuation at $x/b = 94$ (figure 4) increased by 12%, u' by 4% and w' was hardly altered. This case is therefore quite different from the forced mixing layer in which v' was doubled as a consequence of the excitation, w' was halved and u' was hardly increased (Oster & Wygnanski 1982). The present forcing has a major effect on the u'-component in the inner region of the flow at $x/b = 94$ (figures 4*a* and 5*a*) where the local increase in u' was approximately 25% at around $y/y_m \approx 0.6$. At this location the effect of forcing on u' may be compared to the effects observed in the plane mixing

layer where the u' distribution developed a 'saddle point' near the centre of the flow and the Reynolds stress reversed its sign, stopping and even reversing the lateral spreading of the mixing layer (region II in Oster's parlance). Although the analogy between those two cases might have been fortuitous it indicates the need to investigate the detailed energy production and transport mechanisms whenever a negative turbulence production seems possible. The reverse cascade process was considered physically unacceptable and was not thoroughly investigated in the past. The w' component was not increased in the outer part of the flow. The increase in w' was noticeable near the surface but to a much lesser degree than u'. The spanwise component of the fluctuations is not directly produced by straining the mean motion in a two-dimensional flow (unlike the u' component which is directly created by the product $\overline{u'v'}\,\partial U/\partial y$): it is generated by the correlation between oscillating pressure and velocity fluctuations and it thus represents the tendency of the turbulence to become isotropic. Forcing increased the maximum Reynolds stress measured by approximately 10% at $x/b = 94$ but its effect in the inner region of the flow (i.e. at $y/y_m > 0.3$) was minimal (figure 5*d*). One should recall that the $\overline{u'v'}$ correlation could not be measured close enough to the surface and therefore these data are not helpful in assessing the effects of excitation on the skin friction.

The effects of external excitation near the surface become weaker with increasing distance from the nozzle. This might be inferred by comparing the turbulent intensities measured at $x/b = 94$ with those measured at $x/b = 188$ (figures 4 and 5). Significant differences between the u' and v' measured in the excited and in the unperturbed flows were observed at $x/b = 188$ in the region $2.5 > (y-y_m)/y_0 > 1.2$. At $(y-y_m)/y_0 = 2$ excitation increased the level of u' by 30%. One may deduce from this that the external excitation at the chosen St_j initially affected the wall layer by generating or enhancing the coherent structures near the surface. The flow, however, possesses a mechanism which transfers coherent momentum from the inner region outwards at larger x and significantly increases the intensity of the fluctuations in the outer region of the wall jet.

The differences in the turbulent intensities between forced and natural flows are attributed to the coherent motion. By using triple decomposition (see also Hussian 1983 for notation), the time-averaged dimensionless momentum equation takes the form

$$\frac{\mathrm{D}}{\mathrm{D}t}U_i = U_j\frac{\partial U_i}{\partial x_j} = -\frac{\partial P}{\partial x_i} + \frac{1}{Re}\frac{\partial^2 U_i}{\partial x_j\,\partial x_j} - \frac{\partial}{\partial x_j}(\overline{\tilde{u}_{ci}\,\tilde{u}_{cj}} + \overline{u_{ri}\,u_{rj}}),$$

where the instantaneous dimensionless velocity component in the ith direction consists of a mean value U_i, a coherent part $\tilde{u}_{ci}$ and a random part u_{ri}. Thus: $u_i = U_i + \tilde{u}_{ci} + u_{ri}$ where $i = 1, 2, 3$ corresponds to dimensionless u, v and w.

The Reynolds-stress term in this equation is represented by the sum of the coherent and random stresses, and thus the difference between the $\overline{u'v'}$ measured (figure 4*d*) in the forced flow and the $\overline{u'v'}$ measured in the unperturbed flow may represent the additional time-averaged coherent Reynolds stress provided the random stress was not altered by the imposed excitation. One makes the doubtful assumption in this case that the coherent and the random motions are uncorrelated (see Hussian 1983). Regardless of this assumption, the total Reynolds stress is not significantly affected by the presence of the excitation, because the mean flow was not appreciably changed by it. This is in clear distinction to the forced mixing layer where the rate of spread of the flow changed dramatically duc to excitation and most of the stresses observed in regions I and II were coherent (Oster & Wygnanski 1982).

The dimensionless maxima $[(\overline{u_i'^2})_{max}\,v^2/(RJ^2)]$ used for the normalization of $\overline{u_i'^2}$ are

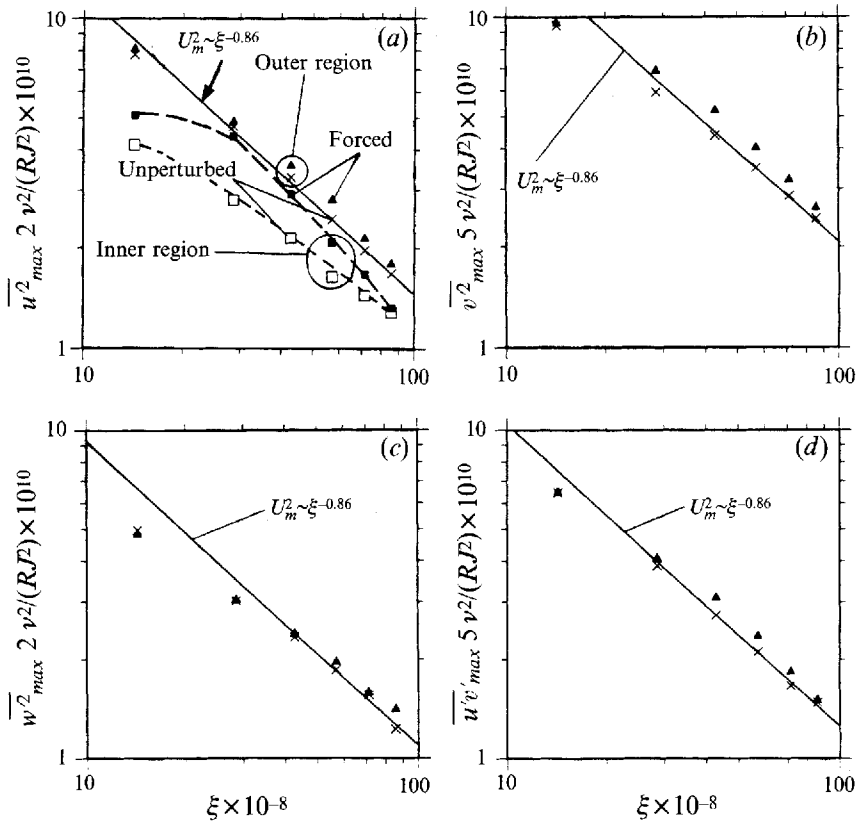

FIGURE 9. The streamwise scaling of the turbulence intensity and the Reynolds stress.

plotted in figure 9(*a–c*) versus the universal streamwise distance $\xi = xJ/\nu^2$ while the maximum shear stress is plotted in figure 9(*d*). The solid lines in these figures represent the decay of the average U_m^2 for the forced and unperturbed flow with ξ. Thus, if the kinetic energy in the mean flow and in the turbulence were in equilibrium and their distribution across the flow were self-similar, the slopes of $\overline{u'^2_{max}}$, $\overline{v'^2_{max}}$, $\overline{w'^2_{max}}$ and of U_m^2 would have been identical. The figure containing the streamwise velocity component (figure 9*a*) indicates clearly that the disparity between the inner and outer intensity scales is not only in magnitude but also in their rate of change with ξ. This reinforces the notion that there are two regions (the wall region and the outer region) in which turbulence is generated at a different rate. External excitation strongly enhances $\overline{u'^2_{max}}$ in the inner region when $\xi \times 10^{-8} < 80$, while increasing it slightly in the outer region at $\xi \times 10^{-8} > 50$ (figure 9*a*). The enhancement of $(\overline{u'^2})$ and $(\overline{v'^2})$ by the excitation is much more obvious in the outer part of the jet (i.e. at $(y-y_m)/y_0 = 2$) than it is at $(y-y_m)/y_0 \approx 0.8$ where $(\overline{u'^2})$ and $(\overline{v'^2})$ have their highest intensity in the absence of forcing (figure 4*a*, *b*). The differences are more significant at large values of ξ. The $(\overline{w'^2})$ component is not affected by the excitation but its rate of change with ξ is different from the other two fluctuating components and from U_m^2. There are clear indications that a stronger excitation at a lower Strouhal number affects the outer region in a more meaningful way (see also KHW).

The coherent part was assumed to be phase-locked to the imposed excitation and traditionally ensemble averaged over a single period of the imposed excitation. This procedure neglects the generation of coherent eddies of lower frequency than the

excitation frequency as well as jitter in the size, shape and advection speed of the coherent structures. The outcome of these assumptions will be discussed later.

2.3. *Higher-order statistical terms and Reynolds-averaged energy balance*

The conventional average budget of turbulent energy (e.g. Tennekes & Lumley 1972) is

$$U_j \frac{\partial}{\partial x_j}(\tfrac{1}{2}\overline{u_i u_i}) = -\frac{\partial}{\partial x_j}\left(\overline{u_j p} + \tfrac{1}{2}\overline{u_i u_i u_j} - \frac{2}{Re}\overline{u_i S_{ij}}\right) - \overline{u_i u_j} S_{ij} - \frac{2}{Re}\overline{s_{ij} s_{ij}}, \tag{2.1}$$

where each quantity is dimensionless and the instantaneous velocity is decomposed into mean and fluctuating components as suggested originally by Reynolds. Namely $u_i = U_i + u_i'$ where $i = 1, 2, 3$, and

$$s_{ij} \equiv \frac{1}{2}\left(\frac{\partial u_i}{\partial x_j} + \frac{\partial u_j}{\partial x_i}\right) \quad \text{and} \quad S_{ij} \equiv \frac{1}{2}\left(\frac{\partial U_i}{\partial x_j} + \frac{\partial U_j}{\partial x_i}\right)$$

represent the fluctuating rate of strain and the mean rate of strain respectively.

The term on the left-hand side of (2.1) represents a rate of change in the turbulent kinetic energy or a transport of turbulent energy by the mean motion. The first term on the right (in parenthesis) represents collectively a transport of turbulence by pressure fluctuations, velocity fluctuations and viscous stresses. The second term on the right represents production of turbulent energy, and the last term dissipation. Not all the components in the energy budget can be measured: the pressure–velocity correlation is the prime example because this term can only be estimated from (2.1) by knowing the other terms. Only some of the terms constituting the dissipation are measurable: the others can be estimated by a variety of assumptions which will be discussed later in the text.

The convection of turbulent kinetic energy to or from a given location in a two-dimensional boundary-layer type of flow becomes

$$\text{Convection} = \tfrac{1}{2}U\frac{\overline{\partial q'^2}}{\partial x} + \tfrac{1}{2}V\frac{\overline{\partial q'^2}}{\partial y}, \tag{2.2}$$

where $\overline{q'^2} = \overline{u'^2} + \overline{v'^2} + \overline{w'^2}$.

Both terms as well as their sum are plotted in figure 10 for the data collected at $x/b = 94$. Most of the influx of turbulent energy occurs at $(y - y_m)/y_0 < 1$ and is associated with the streamwise gradient of $\overline{q'^2}$. The calculated transverse velocity V, which is deemed to be much more accurate than the measured one (see the discussion related to figure 3), changes direction around $(y - y_m)/y_0 = 1.25$ and transports $\overline{q'^2}$ from the wall region and from the outer extremities of the wall jet to the central region of the flow (i.e. where $(y - y_m)/y_0 \approx 1.2$). External excitation increased the maximum gain in the turbulent energy through the convective process by approximately 24% and almost doubled it closer to the surface (see figure 15*b*). Most of this difference stems from an increase in $\overline{\partial q'^2}/\partial x$ near the wall, as might be observed by comparing the data shown in figure 4 for $x/b = 94$ and 188.

Only the diffusion of energy by the turbulent velocity fluctuations was measured here (i.e. the second term in the parentheses on the right-hand side of (2.1)), because the pressure transport can only be estimated from the energy budget itself and the viscous diffusion term is negligible at the Reynolds number considered. The transport terms considered, therefore, are

$$\text{Diffusion} = \frac{1}{2}\left(\frac{\partial}{\partial y}\overline{v' q'^2} - \frac{\partial}{\partial x}\overline{u' q'^2}\right), \tag{2.3}$$

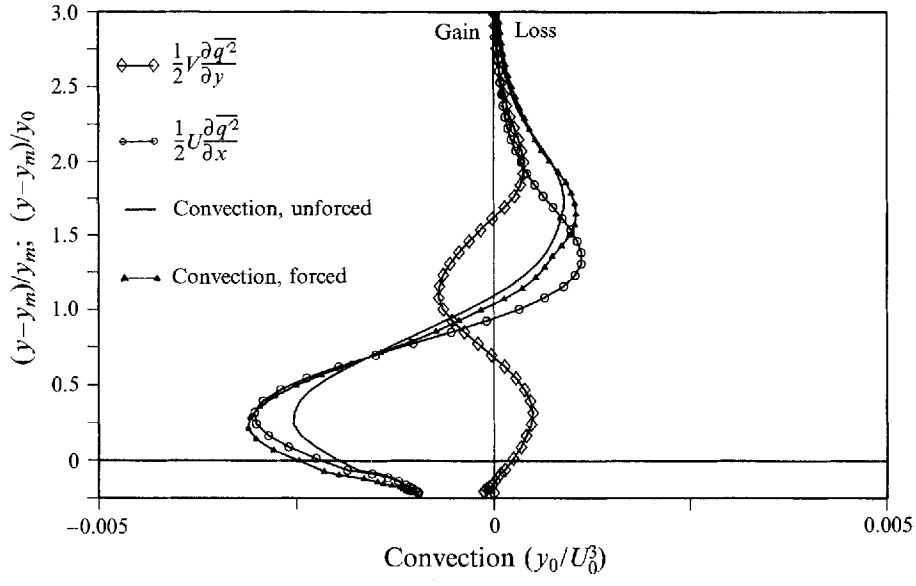

FIGURE 10. The convection term in the energy budget.

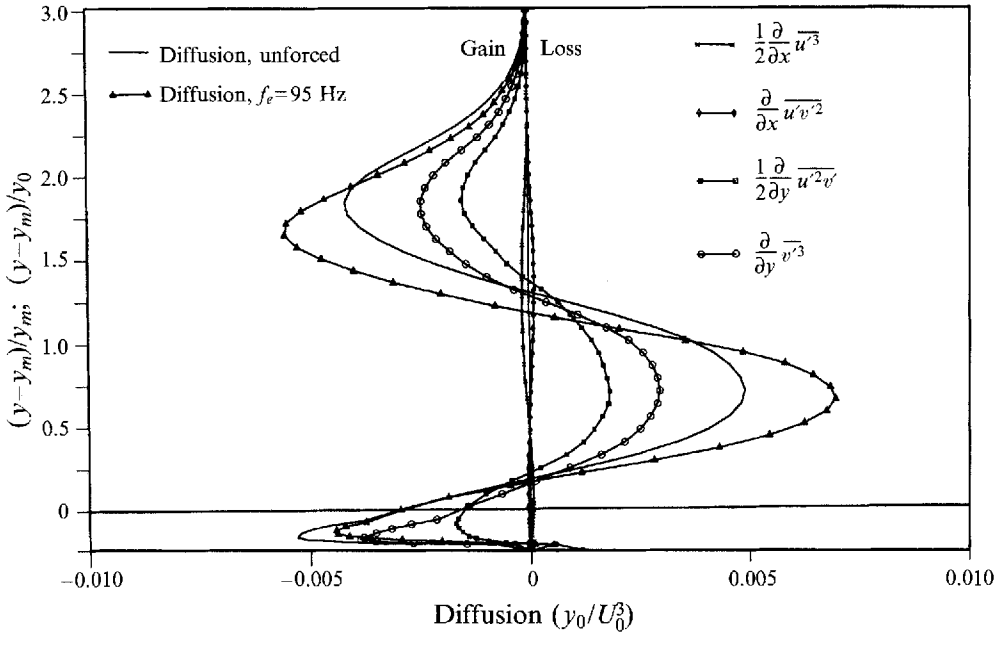

FIGURE 11. The diffusion term in the energy budget.

where the second term is usually negligible in boundary-layer-type flows. Five out of the six terms necessary to estimate the diffusion were actually measured; only $\overline{v'w'^2}$ was assumed to be equal to $\overline{v'^3}$ (such an assumption is common because of the difficulty in measuring $\overline{v'w^2}$ and the similarity between $\overline{w'^2}$ and $\overline{v'^2}$ at $(y-y_m)/y_0 > 0$). The term $\overline{u'w'^2}$ turned out to be equal to $\overline{u'v'^2}$. The turbulent diffusion terms are plotted in figure 11 where it is immediately obvious that the second term in (2.3) is indeed negligible. The transverse velocity fluctuations v' remove energy from the central region of the wall jet and transport it to its extremities. External excitation increases the loss in the

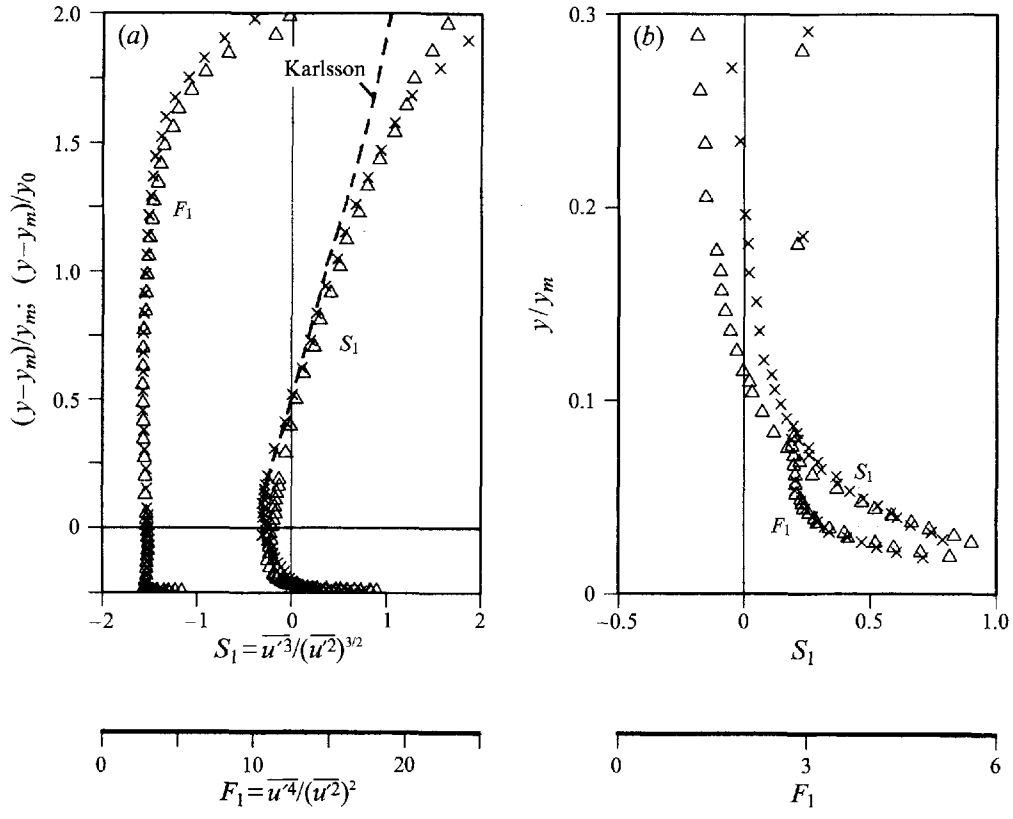

FIGURE 12. The influence of forcing on the skewness and flatness factors.

central region by approximately 40% relative to the unperturbed flow by transporting the energy more efficiently outwards (i.e. towards $(y-y_m)/y_0 = 1.6$). External excitation had little effect on the diffusion near $y = y_m$ but closer to the wall the gain of turbulent energy by diffusion was significantly reduced (figure 15). The maximum energy lost by diffusion occurring at $(y-y_m)/y_0 = 0.7$ is twice as large as the maximum gained by convection at $(y-y_m)/y_0 \approx 0.25$.

Since higher-order correlations give information about the structure of the energy-containing eddies we shall discuss some of them here regardless of their relevance to the energy balance. For example, the skewness $S_1 = \overline{u'^3}/(\overline{u'^2})^{3/2}$ and flatness $F_1 = \overline{u'^4}/(\overline{u'^2})^2$ factors of the streamwise velocity component with and without external excitation are plotted in figure 12. Since the skewness for a Gaussian distribution of velocity fluctuations is zero, it provides information about the symmetry of the fluctuations relative to the local mean velocity. The skewness of the u' component is only slightly negative in the region where the mean velocity is close to maximum; everywhere else $S_1 > 0$. Forcing at the selected frequency did not affect S_1 in the outer region of the flow but it decreased S_1 slightly near the surface. The data in the unperturbed flow are in very good agreement with Karlsson *et al.*'s (1992) experiment, up to $(y-y_m)/y_0 = 1.2$. The discrepancy at $(y-y_m)/y_0 > 1.25$ might be related to the existence of a weak coflowing stream in the present experiment and a recirculation in Karlsson *et al.*'s apparatus.

The values of the flatness factor for a pure Gaussian distribution is equal to 3; deviations from this value are often associated with intermittency γ which is inversely

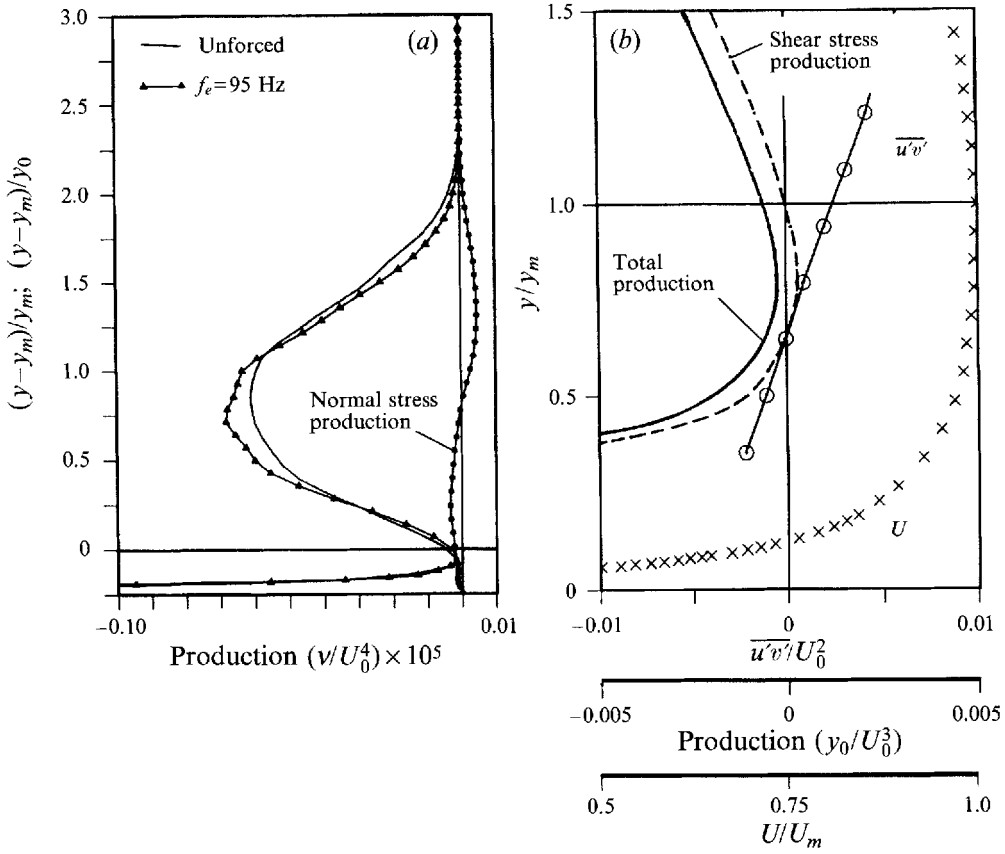

FIGURE 13. The influence of forcing on the production term: (*a*) the entire profile, (*b*) inner layer.

proportional to F_1 (Hinze 1975). According to this criterion the flow became intermittent beyond $(y-y_m)/y_0 = 1.3$. F_1 also increased in the viscous sublayer (i.e. at $y/y_m < 0.04$) but in neither region was it affected by forcing in any meaningful way.

The term representing the production of turbulent energy (the second term on the right hand side of (2.1)) is simplified for two-dimensional mean flow:

$$\text{Production} = (\overline{u'^2}-\overline{v'^2})\frac{\partial U}{\partial x}+\overline{u'v'}\frac{\partial U}{\partial y} \tag{2.4}$$

and is dominated by the product of the shear stress and $\partial U/\partial y$. In fact the maximum production due to the normal stresses is less than 8% of the maximum production due to shear stress in the outer region of the flow (figure 13). The maximum production near the surface is much larger than the maximum production in the outer region because of the steep gradient in the mean velocity. Since $\overline{u'v'}$ changes sign at $y/y_m = 0.6$ there is a possibility that a negative production region exists in the region $0.6 < y/y_m < 1$ before the slope of the mean velocity profile changes sign at $y = y_m$ (figure 13*b*). However, in this region the production due to normal stresses is important and energy is still extracted from the mean motion and passed to the turbulence. This observation is in full agreement with Irwin's (1973) results. Maximum production in the outer region of the wall jet occurs at $(y-y_m)/y_0 = 0.85$ which is further away from the surface than the location at which maximum diffusion loss or maximum convection gain occurs. The turbulent production term is also the largest quantity in the energy

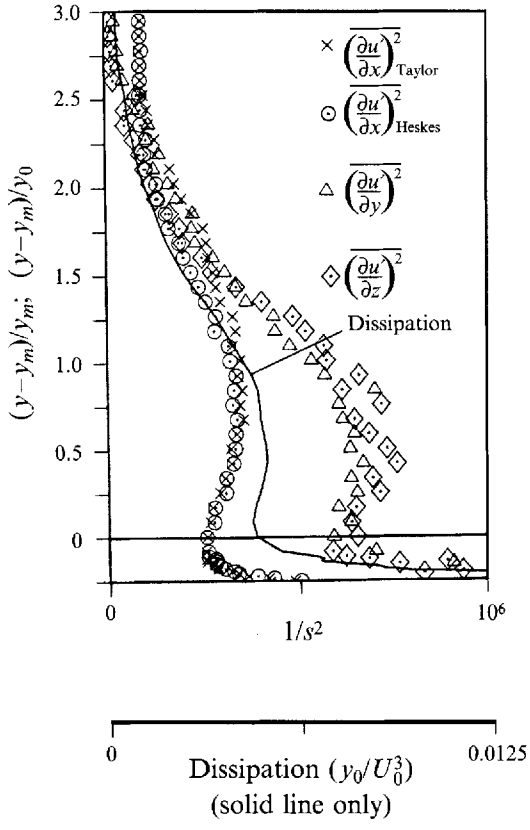

FIGURE 14. The dissipation term in the energy budget.

budget. External excitation increased the maximum production in the outer region by approximately 15% (figure 13).

The dissipation terms (i.e. the last term on the right-hand side of (2.1)) may take the form (Hinze 1975, pp. 188–189)

$$\text{Dissipation} = \frac{2}{Re}\overline{\left(\frac{\partial u_i'}{\partial x_j}\right)^2} \tag{2.5}$$

where the summation notation is applied to both i and j.

Only three of the nine derivatives comprising the dissipation term were measured because the X- and the V-hot-wire arrays were not sufficiently small to resolve the dissipative eddies with any accuracy (in fact they only marginally resolved the energy-containing eddies in the wall region, see above). The streamwise derivative $\overline{(\partial u'/\partial x)^2}$ was obtained from the temporal derivative $\overline{(\partial u'/\partial t)^2}$ by assuming Taylor's hypothesis. Heskestadt's (1965) proposed modification to Taylor's hypothesis hardly affected the estimation of $\overline{(\partial u'/\partial x)^2}$ in the outer region, and both transformations turned out to be identical at $(y-y_m)/y_0 < 1$. The dissipative eddies appear to obey the isotropic relations in the region in which turbulence was not intermittent (figure 14) making $\overline{(\partial u'/\partial y)^2} = \overline{(\partial u'/\partial z)^2} = 2\overline{(\partial u'/\partial x)^2}$. By assuming that the dissipation scales are isotropic all the derivatives in the dissipation term became

$$\overline{\left(\frac{\partial u_i'}{\partial x_j}\right)^2} = 15\overline{\left(\frac{\partial u'}{\partial x}\right)^2}. \tag{2.6}$$

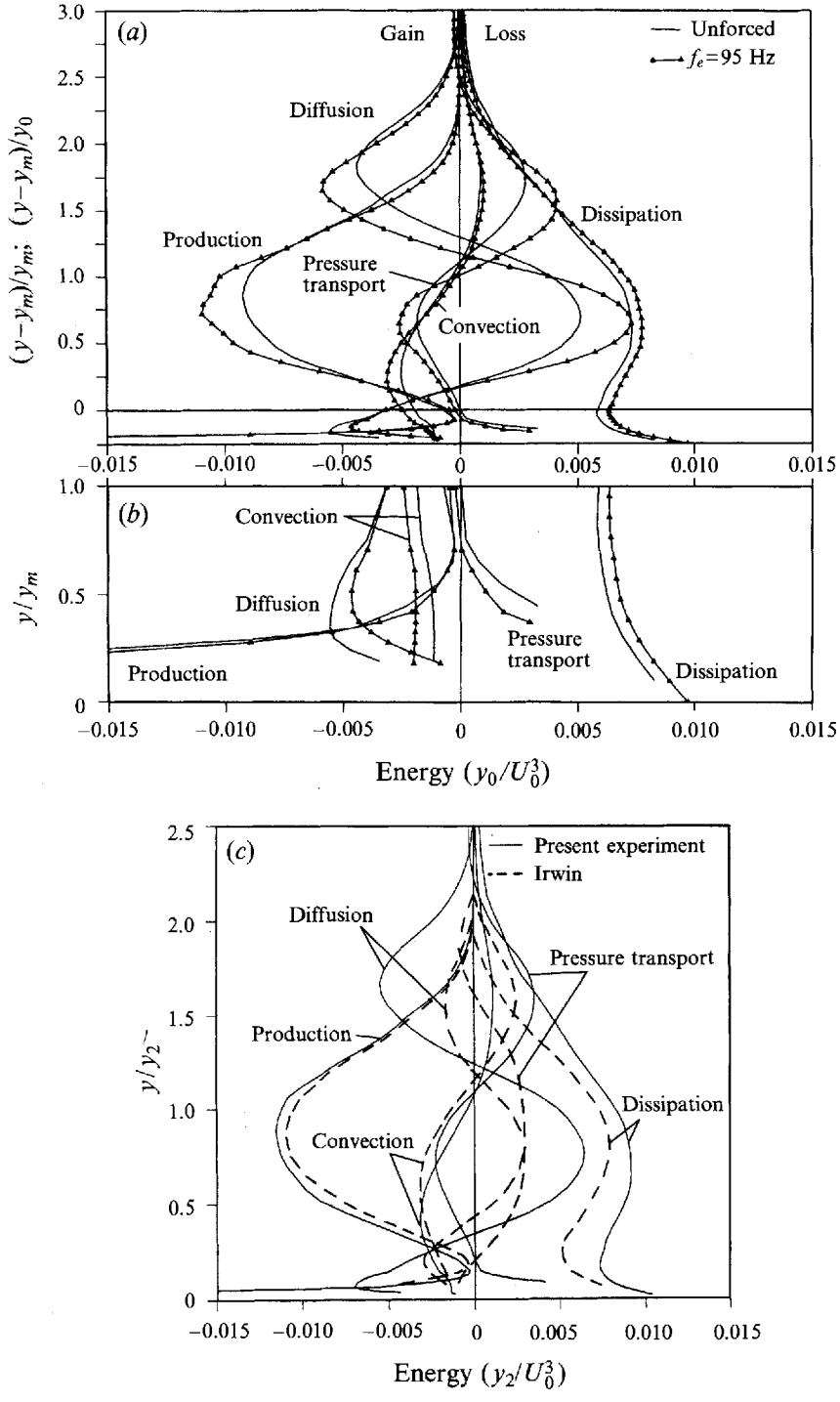

FIGURE 15. The energy budget in the wall jet: (*a*, *b*) influence of forcing, (*c*) comparison with Irwin.

External excitation appears to increase the dissipation terms as well, but this increase is the smallest of all the terms in the turbulent energy budget and amounts to a mere 6% above the dissipation occurring in the unperturbed wall jet.

The pressure–diffusion terms were calculated from (2.1) and the entire balance of turbulent energy is plotted in figure 15. The large-scale transverse motion produced by excitation increased the pressure transport term as well, causing larger loss of turbulent energy in the outer region (at $(y-y_m)/y_0 > 1.25$) and a gain in the central region of the flow around $(y-y_m)/y_0 = 0.8$. The difference in this term due to forcing is very large in the outer region of the flow where it increases the losses by almost a factor of two around $(y-y_m)/y_0 = 1.6$. Transport by pressure fluctuations tends to moderate the transport by velocity fluctuations as the two terms have an opposite sign almost everywhere in the flow. External excitation reduces the turbulent energy production near the surface but it is not visible on the scale of this plot (figure 15*b*); it also reduces the gain caused by velocity diffusion and enhances the dissipation. One may therefore expect a net reduction in the turbulent intensity in this region as the distance from the nozzle increases (figure 4).

One may compare the results obtained here in the absence of excitation with the energy budget compiled by Irwin (1973) for a wall jet in an external stream in a tailored pressure gradient for which a constant ratio of $U_\infty/U_m = 0.38$ was maintained. The production and dissipation terms agree fairly well (figure 15*c*), the advection term is shifted more outwards in Irwin's experiment but the maximum gain of energy by advection is identical in both experiments. This was surprising at first sight because the turbulent intensities measured by Irwin were generally lower (figure 7*a*); however, the rate of decay of U_m with x in Irwin's experiment was larger and the product of those two terms had the observed effect on advection. The two experiments differ in their assessment of diffusion. The velocity–diffusion measured here is twice as large as Irwin's. The differences stem from approximately 12% difference in the r.m.s. values of v' and w' and a smaller difference in u'. As a consequence, the pressure–diffusion terms have generally an opposite sign in the two experiments. It is possible that the slight pressure gradient alters the diffusive transport mechanism in a significant way; unfortunately there are insufficient data to corroborate this supposition.

2.4. *Spectra*

The Reynolds-averaged quantities described provide some information about the effects of external excitation on the turbulent wall jet. They also delineate the regions in the flow in which these effects are significant, but they provide little information about the mechanisms involved and no guidance for active control of the flow.

In order to obtain information about the dominant frequencies of the velocity fluctuations, power spectra of all three velocity components were measured at numerous locations in the flow. Power spectra are a convenient instrument for the identification of large coherent structures and the manner in which those structures scale with other flow parameters. The power spectra of u', v' and w' measured at three dimensionless distances from the surface in the absence of forcing are plotted in figure 16. The ordinate in this figure is normalized to unity while the abscissa represents a dimensionless frequency $\beta = 2\pi f y_0/U_0$. The data presented were taken in the outer part of the flow (figure 16*a*), at the location at which the mean velocity is maximum (figure 16*b*) and near the surface (figure 16*c*). Six curves are plotted on each figure representing data taken at six equal streamwise intervals between $x/b = 31.3$ and 188. The collapse of the normalized power spectra of each component onto a single curve (with the exception of the v' fluctuations near the surface) indicates that the

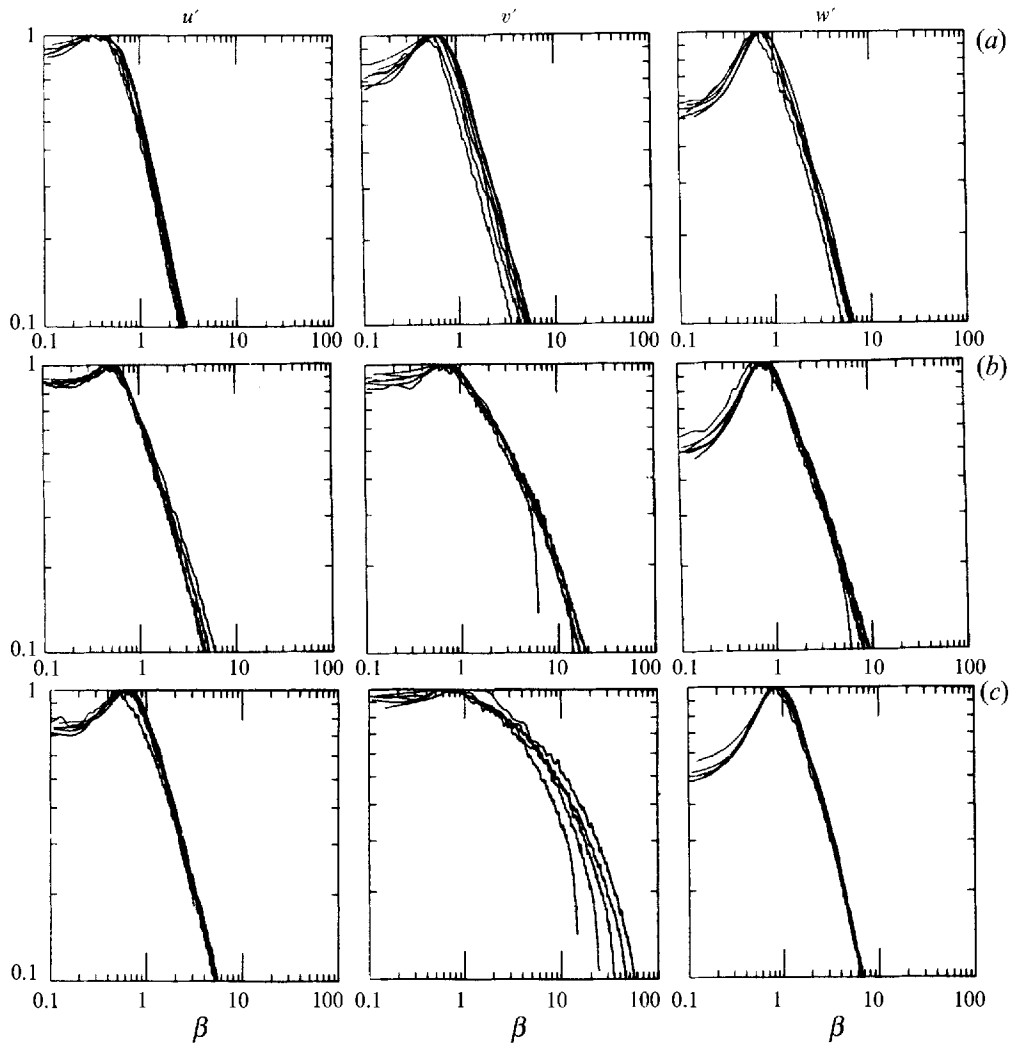

FIGURE 16. Spectra in the naturally developing wall jet: (*a*) in the outer part of the flow, $y-y_m/y_0 = 0.8$; (*b*) at the location of maximum mean velocity, $y/y_m = 1$; (*c*) near the surface, $y/y_m = 0.3$.

predominant frequency in the flow scales with y_0 and U_0. The high-frequency parts of the spectra (i.e. $\beta > 4$) of the v' and w' components are probably incorrect because of the large dimension of the X- and V-hot-wire probes with which those spectra were measured. This factor does not influence the present discussion because only the measurement of the v' component of the spectrum near the surface is affected at its high-frequency end. For this reason we also preferred to assume the existence of isotropy in the dissipative scales rather than rely on measurement of $\overline{(\partial v'/\partial t)^2}$ near the surface.

It is interesting to note that the value of β at which the power spectra of u' and v' attain their maxima depends on the distance from the surface. Far away from the surface $\beta_{max} \approx 0.4$ (figure 16*a*) while near the wall $\beta_{max} \approx 0.7$ (figure 16*c*) for the u' fluctuations and it is somewhat higher for v'. These values of β are between the most amplified and the neutrally stable modes (i.e. those which have gone through the amplification process) calculated for the mean velocity profiles measured, suggesting

that the large structures might have been generated by an instability of the mean velocity field. The coexistence of two distinct frequencies, scaling with the mean flow at all streamwise locations measured, leads one to speculate about the origin of these eddies. Presumably, one originates near the surface while the other near the inflection point of the outer zone, and they may propagate at the same speed and interact in a complex nonlinear fashion. From these data it appears that the frequency ratio between the inner and outer eddies is somewhat lower than two. Zhou *et al.* (1993) who made similar measurements at a variety of Reynolds numbers suggested that this frequency ratio might indeed be an incommensurate number of 1.7. The power spectra of the w' component are almost invariant with y and they all possess a high peak around $\beta \approx 0.8$ suggesting the existence of a dominant spanwise scale.

In the following section we shall not discuss the interaction between the inner and outer coherent structures of the wall jet, but rather the effect of external excitation on the energy transfer between the mean flow and the coherent and incoherent eddies. We have excited the flow at a frequency of 95 Hz (i.e. at $St_j = 9.5 \times 10^{-3}$) corresponding to the most energetic eddies observed near the surface (i.e. corresponding to $\beta \approx 0.7$) at $63 < x/b < 94$. Some of the spectra measured in the flow during excitation are plotted in figure 17. Two sets are shown, one taken at $y = y_m$ and the other at $(y - y_m/y_0 = 0.8$, where the intensity of turbulence was maximum (figure 4). While the imposed fluctuations corresponding to the local peak in the natural frequencies between $x/b = 63$ and 94 were amplified at $y = y_m$, they decayed in the outer region, at the identical streamwise locations. Such an observation has never been made in free shear layers possessing two instability modes (e.g. the plane wake) which were excited by a single frequency. One should recall that at $y = y_m$ a strong interaction between the eddies originating in the wall zone and eddies originating in the outer zone occurs.

It should be emphasized that the absence of sharp peaks in the power spectrum of a specific velocity component is not a sufficient condition for the non-existence of coherent structures. First, in the absence of forcing the spectral peaks are fairly broad. Furthermore, as the present experiment indicates (figure 17*b*), there is no peak in the power spectrum of the u' component in the outer part of the forced wall jet at $x/b \geqslant 94$, while such peaks do exist in the v' component. It also appears that beyond $x/b = 94$, a strong but a broad peak in the power spectrum of the v' component develops in the low-frequency region and it persists through the remaining distances measured (probably even beyond $x/b = 188$), across the entire wall jet (figure 17*c*, *d*). Between $x/b = 94$ and 125 this peak occurs at the subharmonic of the forcing frequency but beyond that distance, after the fundamental decayed and disappeared from the outer region, it became proportional to the characteristic length and velocity of the jet (i.e. the value of β corresponding to this peak remained constant). Is this peak a manifestation of a coherent motion, phase-locked initially to the imposed oscillations, or is it merely a random, low-frequency component? In order to answer this question one has to establish quantitatively what is meant by 'coherent motion'.

The coherence spectra were calculated from the data obtained by two probes separated in the spanwise direction by a distance Δz. The conclusions based on the coherence in the present experiment were identical to the observations of KHW and will therefore not be discussed in detail. The forced flow responds to the two-dimensional excitation from the nozzle with coherence values approaching unity even at large streamwise distances and fairly large Δz (see also figure 21 of KHW). It implies that the imposed two-dimensional perturbations do not lose their identity far downstream.

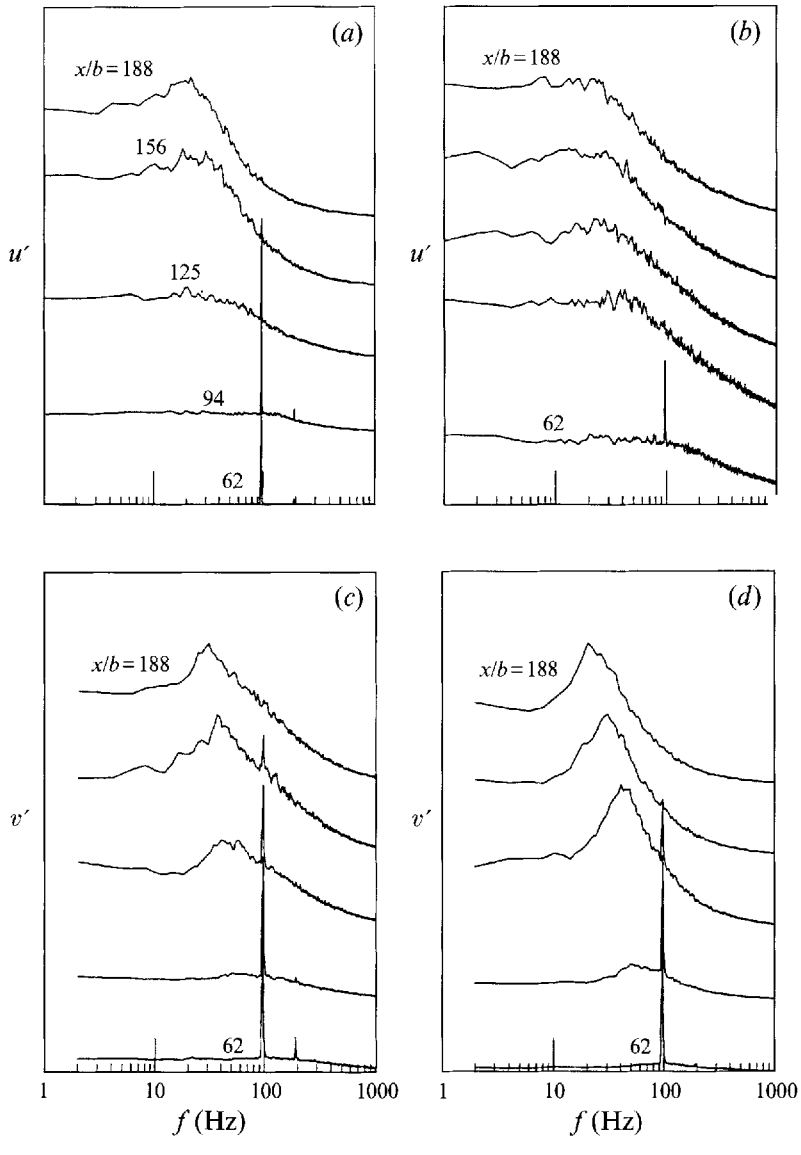

FIGURE 17. Spectra in the forced wall jet: (*a*) u' at $y/y_m = 1$, (*b*) u' at $(y-y_m)/y_0 = 0.8$, (*c*) v' at $y/y_m = 1$, (*d*) $(y-y_m)/y_0 = 0.8$.

2.5. *Triple decomposition*

Thus far, we have decomposed the equations of motion into mean and fluctuating components and analysed the flow in those terms regardless of forcing. Periodic excitation of the flow provides a phase reference which enables one to examine the significance of the coherent phase-locked component as well. Excitation, in this case, does not only modulate the flow but interacts with it. To some extent it reorganizes the coherent motion existing naturally in the flow and enhances it. External excitation, therefore, is not only a diagnostic tool but also a tool which manipulates and controls the flow.

Any instantaneous variable of the flow can be decomposed into three constituents: time-independent, coherent and random (Hussain 1983). Thus the instantaneous

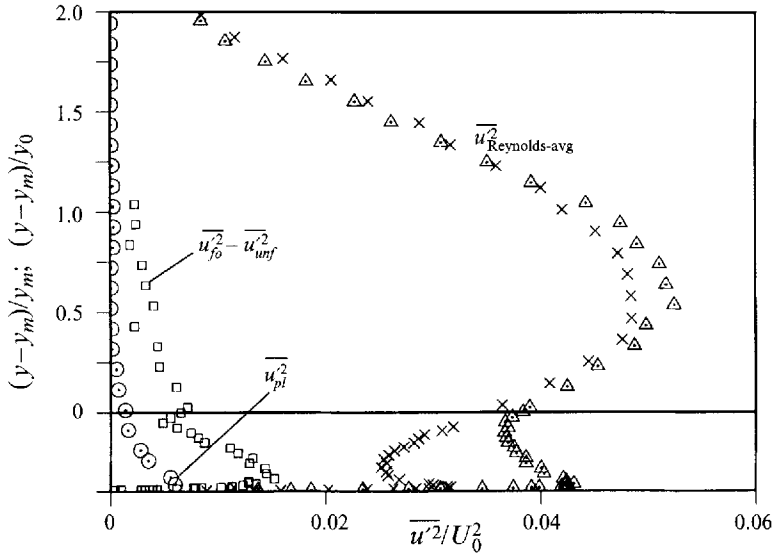

FIGURE 18. The comparison between increment of turbulence intensity caused by forcing with the phase-locked intensity at $x/b = 94$.

streamwise velocity component in a two-dimensional steady mean flow may be written as

$$u(x, y, t) = U(x, y) + \tilde{u}_c(x, y, t) + u_r(x, y, t), \tag{2.7}$$

where the temporal average of u is $\bar{u} = U$ while its phase-locked average part is traditionally defined as $\langle u \rangle = U + \tilde{u}_c$. As pointed out by Hussain (1983), the triple decomposition is a formalism for a quantitative discussion of coherent structures (e.g. the energy contained by coherent structures) but it is not free of ambiguities and assumptions embedded in the terminology of phase-locked averaging and its relation to coherent structures. We shall address them in this section, but before doing so let us demonstrate the need for the triple decomposition.

One may assume that the coherent energy of any fluctuating velocity component, say u, is merely the difference in the energy calculated by applying the classical double decomposition $\overline{(u-U)^2}$ to the flow under investigation twice: once with external excitation and once without it. Such an assumption lumps together all the nonlinear processes generating and organizing coherent modes as well as the processes distorting the mean flow. For example, the intensities of the streamwise fluctuations measured by $x/b = 94$ with and without excitation are replotted in figure 18 after being normalized by the unperturbed lengthscale and velocity scale. In this way the different mean kinetic energy content of the flow, caused by differences in skin friction, spreading rate or plane distortion of the velocity profile is accounted for. In addition the phase-locked ensemble-averaged intensities $\overline{(u_c'^2)_{pl}} \equiv (\langle u \rangle - U)^2$ are also plotted on this figure, where the perturbations resulting from a single period of the imposed excitation were repeatedly ensemble averaged to form $\langle u \rangle$. The quantity $[\overline{(u')^2_{forced}} - \overline{(u')^2_{natural}}] > \overline{(u_c'^2)_{pl}}$ and it is not clear if the discrepancy stems from a poor definition of $\overline{(u_c'^2)_{pl}}$ which may misrepresent the intensity of the coherent structures. Other questions affecting the above inequality may also be raised: How strong are the coherent structures existing in the unperturbed flow? How much random energy is organized by the forcing and turned into coherent motion? Does the phase-locked intensity really represent the coherent eddies? All of these reflect on the need for further exploration based on triple decomposition.

At first sight, phase-locked averages should enable us to differentiate between the coherent and incoherent motion for the periodically excited flow. The random component of the fluctuations may be obtained by subtracting the phase-averaged quantity for each period of forcing from the instantaneous data, while the intensity of the coherent motion is given by $\overline{(u_c'^2)}_{pl}$. Although this procedure is statistically valid it underestimates the strength of the coherent motion because it neglects the generation of all coherent subharmonics and the inevitable phase jitter among all the coherent waves. In analysing artificially induced turbulent 'spots' in a laminar boundary layer Glezer, Katz & Wygnanski (1989) observed that the subtraction of an ensemble-averaged signal from a single event resulted in a physically erroneous estimate of the 'random' motion. Thus a procedure was developed which separated the coherent motion from the incoherent one for each triggered event. Wygnanski, Haritonidis & Kaplan (1979) used pattern recognition techniques in order to educe a turbulent 'spot' from a background turbulent boundary layer. We thus set out to develop a quantitative definition of coherent motion after recognizing that it is not represented by phase-locking the data to the imposed oscillations. However, since the forcing signal is periodic, the conditions for distinguishing between coherent and random fluctuations are set up in Fourier space.

The various techniques used to identify the coherent constituents of the turbulent motion can be divided into two categories: in one category the phase relationship (i.e. the phase-locked ensemble-averaging procedure) is the dominant feature, while in the other the identification of spatial scales dominates. The VITA technique (standing for Variable Interval Time Average, Blackwelder & Kaplan 1972) for example, accentuates the phase locking of a recognizable pattern while disregarding the significance of its scale. Other techniques average the scale and the time of occurrence of the repeated observations (e.g. Wygnanski *et al.* 1979). It was determined that the traditional phase-locking and ensemble-averaging procedure underestimates and at times even obliterates the coherent constituents of the turbulent motion in the wall jet owing to the phase jitter associated with the largest scales of the motion. Thus, any practical definition of coherent motion has to accommodate the presence of jitter.

The technique adopted to analyse hot-wire data is an extended pattern-recognition technique which avoids the problem of phase jitter in the recorded time series. Typical pattern-recognition schemes represent the motion by a sum: $\Sigma a(t)\,c(x)$ where $c(x)$ is the spatial basis and $a(t)$ is the time-dependent coefficient. It is used to process instantaneous information in the entire space (e.g. images obtained using particle image velocimetry or flow visualization); however, it is not convenient for processing temporal information generated at a point in space as provided by a hot-wire probe. In this case the decomposition $\Sigma c(x)\,a(t)$ where $a(t)$ is the temporal basis and $c(x)$ is the spatially dependent coefficient is more appropriate. In both procedures it is important to determine the minimum number of terms that represent most of the complex dynamics involved.

Our procedure starts with a Fourier expansion of the time series describing velocity. The physical modes chosen as a start are the eigenfunctions of the anticipated instabilities. In principle, any signal representing a turbulent motion by a limited total sampling period consisting of a discrete agglomeration of waves is the summation of all the Fourier components:

$$u' = \sum_{n=0}^{\infty} [A_n \sin(n\omega t) + B_n \cos(n\omega t)], \tag{2.8}$$

where $n = 0$ corresponds to the time-independent constituent, $\omega = 2\pi/T$, and T is the

total sampling period of the signal which should be chosen as a large multiple, n_0, of the fundamental forcing period. One may expect that the signal of the coherent constituent can be approximated by a truncated Fourier expansion:

$$u_c = \sum_{n=0}^{n_{max}} [A_n \sin(n\omega t) + B_n \cos(n\omega t)], \tag{2.9}$$

where n_{max} corresponds to the harmonics of the highest frequency regarded as coherent. The Fourier components with frequency higher than n_{max} can be regarded as representing random small-scale motion. By noticing that the total sampling period is an integer multiple n_0 of the fundamental forcing period, the above expansion can be expressed as

$$u_c = \sum_{n=0}^{n_{max}} \left[A_n \sin\left(\frac{n}{n_0}\omega_0 t\right) + B_n \cos\left(\frac{n}{n_0}\omega_0 t\right)\right], \tag{2.10}$$

where $\omega_0 = n_0 \omega$ is the fundamental forcing frequency.

We observed that only those components with $n/n_0 = (2)^{\pm k}$, $k = 0, 1, 2, 3, \ldots$, are of significance and thus

$$u_c = \sum_{k=k_{min}}^{k_{max}} [A_k \sin(2^k \omega_0 t) + B_k \cos(2^k \omega_0 t)]. \tag{2.11}$$

The key point of this method is the application of a pattern-recognition technique in the time domain to all the Fourier components of interest, i.e. applying the Fourier transformation to the individual realizations of the corresponding patterns instead of the entire duration of the signal. For this purpose, the time series are subdivided into segments containing the minimum number of waves sufficient for the pattern of interest to be conserved. Such a segmentation is only possible when the velocity and the imposed oscillations are recorded simultaneously on a long continuous record, as it is done for the purpose of obtaining the traditional phase-locked ensemble-averaged data. For example, one wave of the excitation is contained in each segment representing the fundamental (forcing) frequency in the pattern with its higher harmonics, two waves are in each segment for the subharmonic frequency, four waves for the second subharmonic frequency etc.... Only then is the ensemble-averaging procedure used. This 'chopping' of signals is necessary since any longer segmentation (containing, say, two of the sought waves per segment) will smear out a portion of the 'coherent' pattern because it will not make a proper allowance for jitter between adjacent waves contained in the same segment.

Consider the case (figure 19*a*) where the amplitude of the fundamental wave is extracted from the individual segments of the original time series whose duration corresponds to the period of the excitation. In this case the first Fourier coefficient of each transformed segment was ensemble averaged to yield the resulting amplitudes. However, when one evaluates the amplitude of the fundamental wave derived from a segment that is one wave long and one compares it to the amplitude derived from segments twice as long, one discovers that the former is reduced by approximately 50% over most of the wall jet (figure 19*a*). One may continue this procedure by extracting the Fourier coefficients corresponding to the fundamental frequency from longer and longer segments of the original time series and observe a progressive reduction in the perceived amplitude of this wave. In the limit, this procedure tends to the conventional eduction technique in which the first Fourier coefficient is obtained from a phase-locked and ensemble-averaged signal whose duration is equal to a single period of the excitation. The difference in the amplitude of the coherent structure educed by changing the sequence of the procedure is attributed to a phase jitter between the

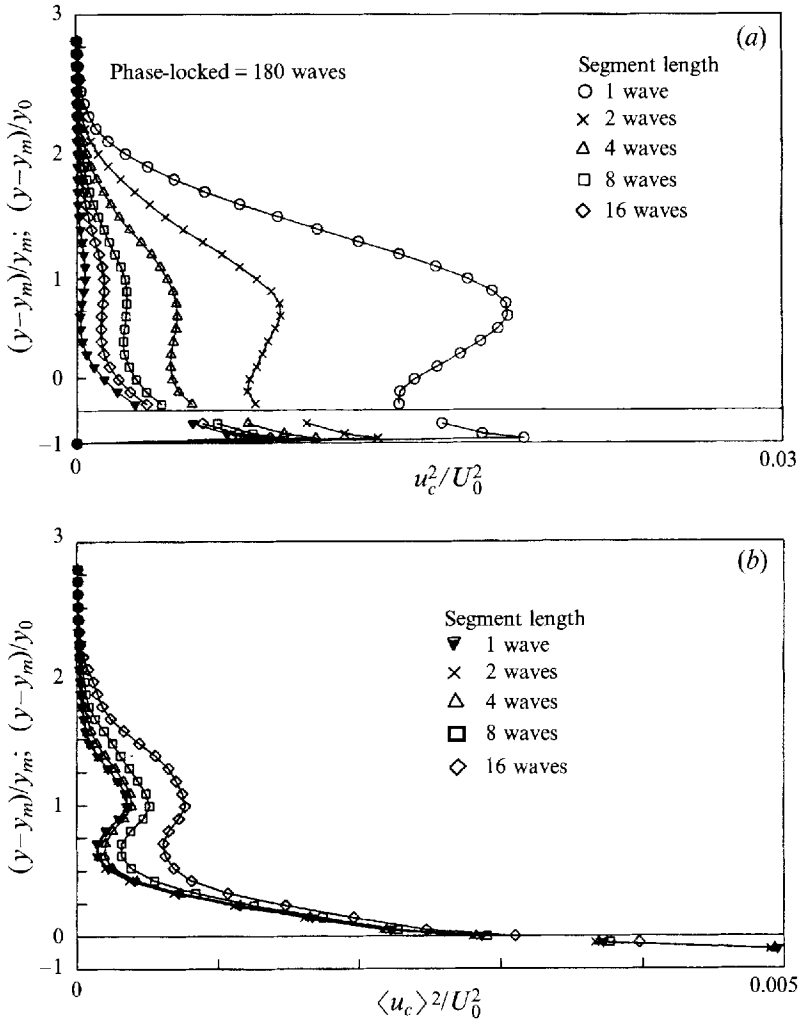

FIGURE 19. The influence of the number of waves in each segment on the estimated turbulence intensity: (*a*) using the new technique, (*b*) using ensemble-averaged data.

forcing signal and the velocity perturbation representing the coherent wave evoked by it. Thus, by taking segments whose duration corresponds to two or more wavelengths of the forcing frequency, one requires that the phase between the consecutive waves in each segment be fixed. It results in a perceived loss of amplitude due to partial cancellations of phase-shifted waves (figure 19*a*). The jitter is less noticeable near the surface where the amplitude of the fundamental educed from a segment 16 waves long was only decreased to 45% of the amplitude derived using segments one wave long.

Traditionally, the existence of the coherent subharmonic was verified by breaking the continuous record into segments whose period was twice the period of forcing before ensembling them, and extracting the appropriate Fourier coefficient from the ensemble-averaged signal. One may also educe the amplitude of the fundamental from this signal and observe that it is slightly larger than the amplitude educed from a shorter sample. One may apply the procedure to longer samples which will somewhat relax the constraint on the jitter and yield larger amplitudes of the fundamental wave (figure 19*b*). The phase-locking and ensembling of segments of a finite duration will

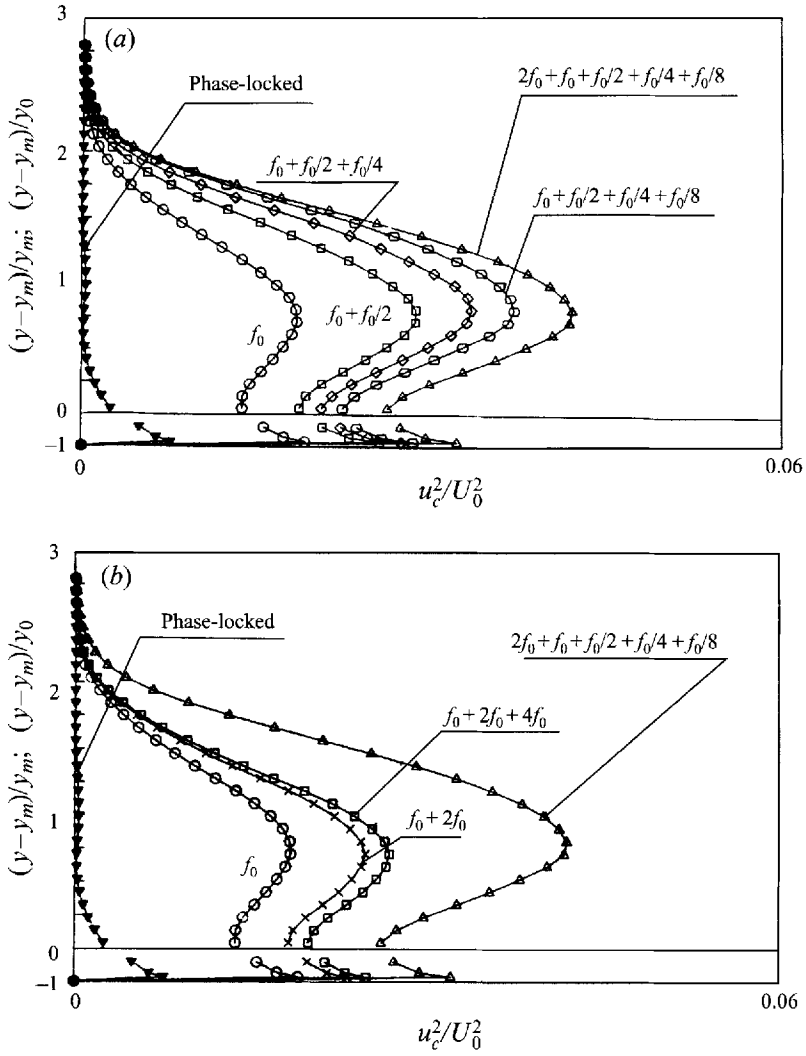

FIGURE 20. The influence of the number of Fourier components on the estimated turbulence intensity: (*a*) subharmonics, (*b*) higher harmonics.

always have jitter which will smear out and reduce the amplitude of the perceived coherent motion. This exposes the shortcoming of the conventional ensemble-averaging procedure. The difference between the two methods of processing the data is very large in the outer part of the flow.

The overall energy of a coherent motion consisting of a discrete agglomeration of waves is the summation of all the above-mentioned Fourier components of significance. Consider the various subharmonics of the fundamental frequency and determine the energy contained in an ever-increasing summation of terms $\Sigma_{n=1}^{\infty}\overline{(u')^2_{f_0/n}}$. These series converge fairly rapidly so that the difference between a summation over three terms and four terms is less than 10% of the larger sum (figure 20*a*). One may, of course, consider the various intermediate frequencies like $\frac{3}{4}/f_0$, $\frac{3}{8}/f_0$, etc., but those did not appear to contribute significantly to the overall energy of the coherent motion. The fundamental frequency alone accounts for only 35% of the four-term sum which was chosen as a representative quantity of the large coherent motion.

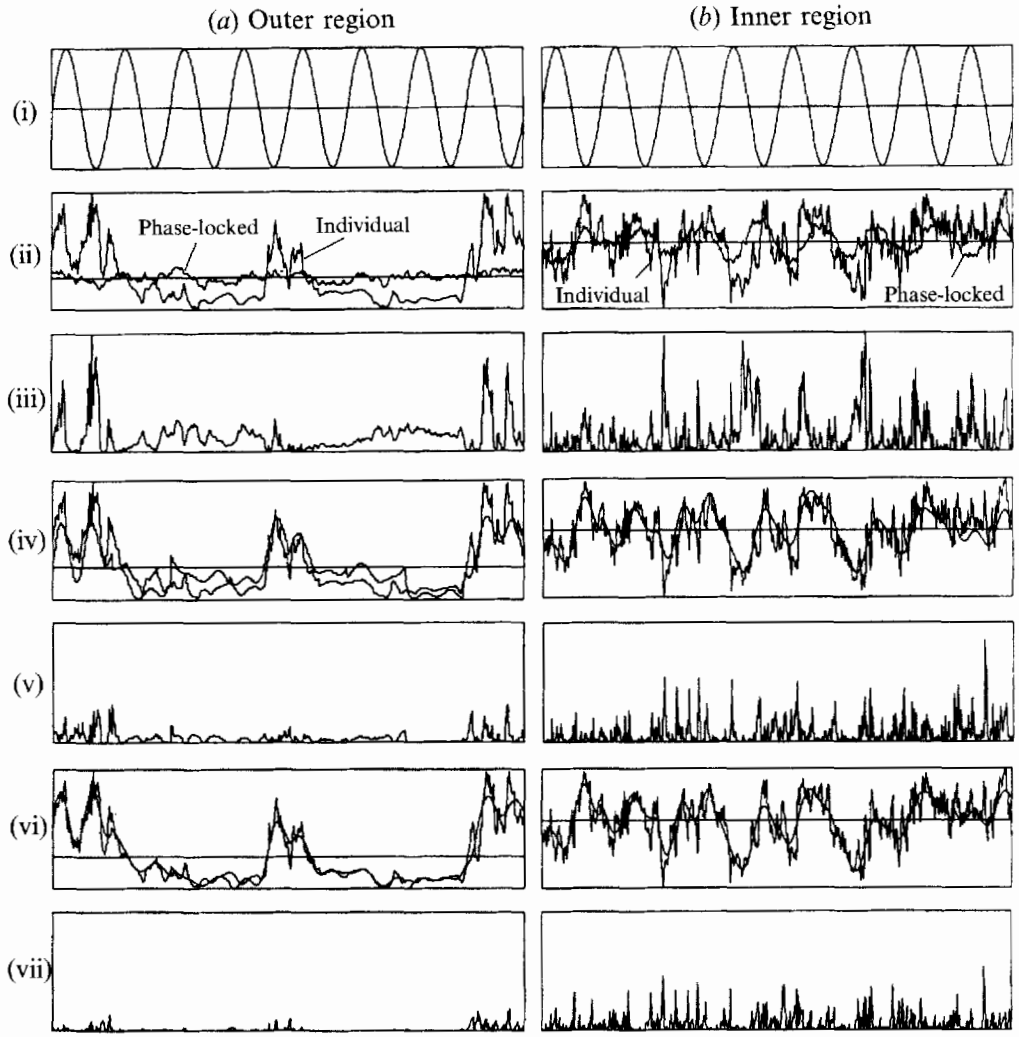

FIGURE 21. A demonstration of the influence of the low-frequency subharmonics on the reconstructed coherent wave form: (*a*) outer region, (*b*) inner region. For description of (i) to (vii) see text.

One may also consider the addition of various harmonic frequencies which are always present when the fundamental wave attains a finite amplitude

$$\sum_{n=1}^{\infty} \overline{(u')^2_{nf_0}}.$$

The inclusion of the first harmonic, $2f_0$, adds approximately 14% to the four-term summation of waves equal to or larger than the fundamental while the inclusion of the second harmonic $4f_0$ adds already less than 5% to this summation (figure 20*b*). We thus conclude that a reasonable representation of the coherent energy in this case is achieved by using a five-term series (including the first harmonic $2f_0$) to represent the intensity, $\overline{u_c^2}$, of the coherent motion in the wall jet (figure 20).

It is clear that the definition of coherent eddies should directly affect the intensity of the random ones. The significance of the adopted procedure is illustrated in the two examples given in figure 21, where (*a*) is taken in the outer region of the wall jet (at

$y/y_2 = 1.27$) while (*b*) is very near to the surface ($y/y_m = 0.1$). Eight periods were used in the phase-averaging procedure for the purpose of the present demonstration, and consequently eight waves of the imposed oscillation are plotted in figure 21(*a*)(i). An individual time record of the velocity is plotted in (ii) together with a conventional, phase-locked and ensemble-averaged record of some 20 events. The difference between the two records squared (i.e. $(u-\langle u\rangle)^2$) is plotted further in (iii) and represents the random part of the velocity fluctuations defined in a conventional way. One may infer from this example that most of the fluctuating energy is probably random because it appears to be an order of magnitude larger than the coherent energy. For comparison, one may represent the large coherent structures by using only a small number of leading Fourier coefficients (say $\frac{1}{2}/f_0$, f_0 and $2f_0$ as discussed above) and abandon the precise phase relation between the forcing signal and the longer velocity record. The velocity signal may then be reconstructed from each record of duration $t = 8/f_0$ in (iv). There is a major improvement in this representation over the conventional ensemble average plotted above. This is particularly true during the first cycle of the excitation (plotted on the left-hand side of the figure) where the 'random' intensity of the fluctuations was reduced by approximately a factor of 4 (v). Applying the same procedure to this signal but using two additional terms, $f_0/4$ and $f_0/8$, represents the low frequencies of this instantaneous record very well (vi). In this case, the random intensity of the fluctuations was reduced by an order of magnitude (vii). There is hardly a presence of $f_0/4$ near the surface (figure 21*b*) and therefore a three-term Fourier representation consisting of $f_0/2, f_0$ and $2f_0$ would have been sufficient. In fact, even the conventional ensemble average represents the coherent flow fairly well, suggesting that the jitter is much smaller in this region. Nevertheless, even here the amplitude of the coherent motion is enhanced by the new procedure at the expense of the random fluctuations. Although there is no need for lower frequencies in assessing the coherent motion near the surface (e.g. figures 21*b* and 20*a*) a uniform procedure containing a series of five terms and including $f_0/4$ and $f_0/8$ was used in processing the data.

Since the original time series were segmented into short records containing a few periods of the forcing frequency, $\overline{u_c} \neq U$ for every segment. The difference, which appears in the zeroth coefficient of the Fourier series represents a jitter of the mean velocity per segment. It may stem from the existence of very low frequencies in the flow (i.e. frequencies lower than the ones corresponding to the length of the segment). The total intensity measured by using double decomposition $\overline{u'^2}$, the coherent intensity $\overline{u_c^2}$, the random intensity $\overline{u_r^2}$ and the jitter intensity calculated by the new procedure are plotted in figure 22. The results indicated that the total intensity equals the sum of the coherent intensity, the random intensity and the jitter. Thus, the resultant jitter can be estimated by

$$\overline{u_j^2} = \overline{u'^2} - (\overline{u_c^2} + \overline{u_r^2}). \tag{2.12}$$

Actually, the jitter intensity is the remainder of the data processing procedure. It is largest around $(y-y_m)/y_0 > 1$ where there is a strong presence of very low frequencies (figure 21). Physically, it can be further divided into coherent and random parts. The coherent part includes the subharmonic frequencies lower than those accounted for in the calculations of the coherent intensity. The rest of the jitter may belong to the low-frequency random fluctuations. However, in practice we may regard the jitter as yet another portion of the random motion as long as the selected number of Fourier components is sufficient to represent the coherent motion. Although in the conventional definition of the average intensity of the phase-locked coherent structures $\overline{(u_c^2)_{pl}} = \overline{(\langle u\rangle - U)^2}$, jitter intensity does not appear explicitly, it was embedded in the phase-locked procedure and cancelled a significant portion of the coherent intensity. Thus the

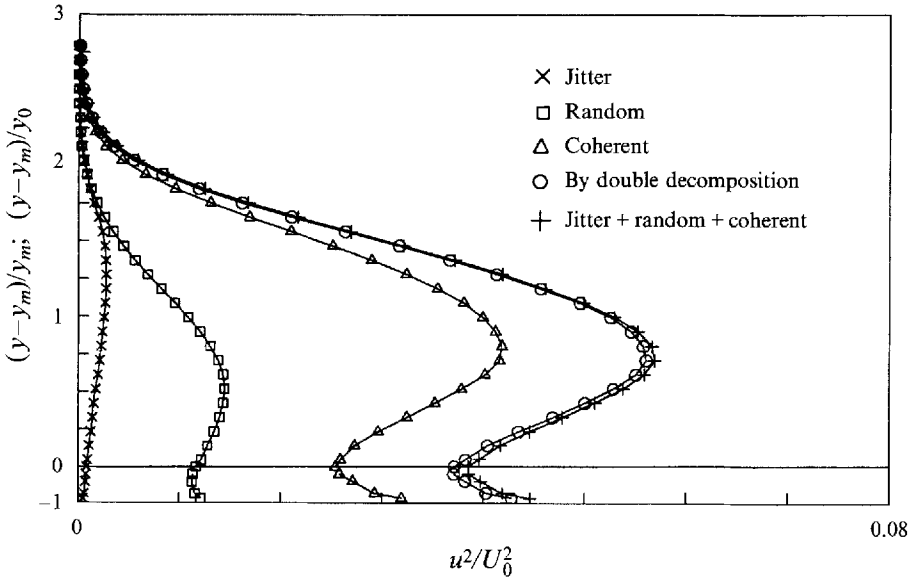

FIGURE 22. The significance of jitter.

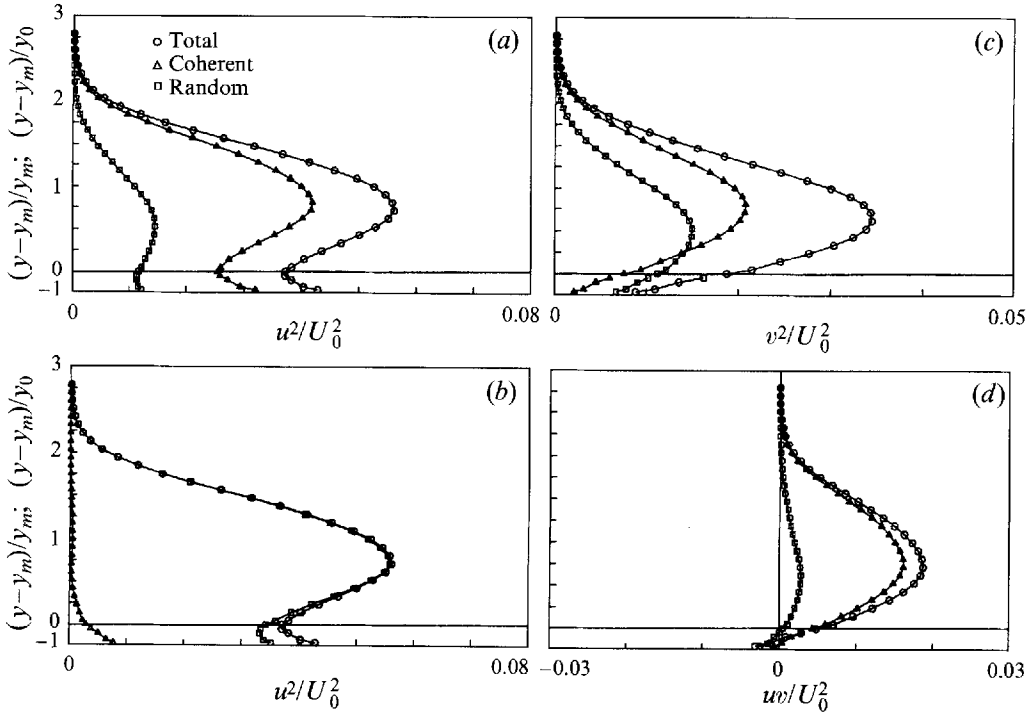

FIGURE 23. The comparison between the new procedure and the conventional phase-locked ensemble-averaged data. (*a*) Streamwise component of turbulence intensity – new procedure; (*b*) streamwise component of turbulence intensity – conventional procedure, (*c*) normal component of turbulence intensity – new procedure, (*d*) Reynolds stress – new procedure.

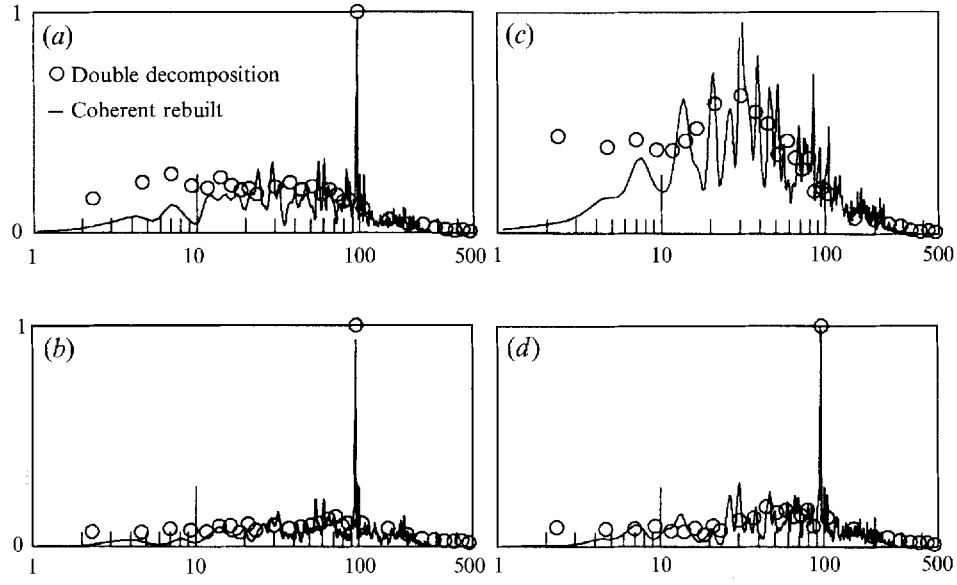

FIGURE 24. A comparison between the reconstructed spectra representing the coherent motion and the low-frequency measured ones. (*a*) u' at $y/y_m = 1$, (*b*) v' at $y/y_m = 1$, (*c*) u' at $(y-y_m)/y_0 = 0.8$, (*d*) v' at $(y-y_m)/y_0 = 0.8$, $f_0 = 95$ Hz, $x/b = 94$.

conventional phase-locked ensemble-averaged intensity cannot be considered as a proper definition of the coherent motion.

A comparison between $\overline{u_c^2}$ obtained by taking five Fourier coefficients using the new procedure and $(\overline{u_c^2})_{pl}$ obtained by the conventional phase-locked ensemble-averaging procedure is shown in figure 23(*a*, *b*). The $\overline{u_c^2}$ estimated by the new procedure which minimized the influence of jitter accounts for 75% of the overall intensity of the streamwise component of velocity $\overline{u'^2}$ at all y-locations, while the intensity of jitter and the intensity of the random fluctuations combined account for approximately 25% of the energy at $x/b = 94$ (figure 23*a*). The distribution of $(\overline{u_c^2})_{pl}$ across the wall jet is plotted underneath for comparison. It is unreasonably small (figure 23*b*) beyond $y/y_2 > 0.5$ and attains a maximum value of 20% of the total $\overline{u'^2}$ near the surface. Most of the turbulent intensity of $\overline{u'^2}$, based on the phase-averaged data, would thus be considered as random. It is clear that a slight jitter in the relative phase of coherent fluctuations can reduce the perceived intensities of those fluctuations by an order of magnitude and, thus, the new procedure appears to be much more reasonable.

The normal component of the coherent velocity fluctuations account for 60% of the total $\overline{v'^2}$ (figure 23*c*) while the coherent shear stress accounts for 85% of the total $\overline{u'v'}$ (figure 23*d*). Since external excitation did not have any effect on the absolute intensity of $\overline{w'^2}$ only its average values were stored and thus the existence of $\overline{w_c'^2}$ in the wall jet remains unknown. The order of magnitude of the coherent motions estimated by these results are consistent with the common observation in forced free shear flows.

One may think that a very large number of terms would be required to represent the low-frequency portion of the spectrum plotted in figure 17. We therefore attempted to reconstruct this part of the continuous spectrum by using the five frequencies representing the coherent structures and the low-frequency jitter. To our surprise, the reconstructed spectra contained the most important features observed (figure 24). The u' spectrum at $x/b = 94$ contained no peak at the forcing frequency in the outer part of the flow but had one at $y/y_m = 1$. The v' spectra contained a peak at the forcing

frequency f_0 at all locations. There is no peak at $f_0/2$ in either u' or v' spectra although the inclusion of this frequency in the definition of coherent structures essentially doubled the intensity of this motion (figure 20*a*). It is also surprising that only one distinct pack in the spectra is observed in figure 24 although five frequencies were used to represent them. The measured spectra (marked by open circles in this figure) are smooth while the reconstructed ones are jagged. This is the main difference between the two and is attributed to 'detuning' caused by random high-frequency fluctuations. The fact that the reconstructed spectra are not as peaky as we thought they ought to be is attributed to phase jitter.

2.6. *The kinetic energy budget for the coherent eddies*

The above definition of the coherent motion enabled us to get a partial estimate of the average kinetic energy balance for the coherent flow by using the triple decomposition formulation of Hussein (1983):

$$U_j\frac{\partial}{\partial x_j}(\tfrac{1}{2}\overline{u_{ci}\,u_{ci}}) = -\frac{\partial}{\partial x_j}(\overline{u_{cj}\,p_c}+\tfrac{1}{2}\overline{u_{ci}\,u_{ci}\,u_{cj}})-\overline{u_{ci}\,u_{cj}}\frac{\partial U_i}{\partial x_j}$$
$$+\overline{\langle u_{ri}\,u_{rj}\rangle}\frac{\partial u_{ci}}{\partial x_j}-\frac{\partial}{\partial x_j}\overline{u_{ci}\langle u_{ri}\,u_{rj}\rangle}-\bar{\epsilon}_c, \tag{2.13}$$

where $u_i = U_i+u_{ci}+u_{ri}$, $i = 1, 2, 3$;

$$\bar{\epsilon}_c = \frac{2}{\mathrm{Re}}\overline{s_{cij}\,s_{cij}} \quad \text{and} \quad s_{cij} \equiv \frac{1}{2}\left(\frac{\partial u_{ci}}{\partial x_j}+\frac{\partial u_{cj}}{\partial x_i}\right).$$

The viscous diffusion term and the production due to normal stresses were neglected in (2.13) because both terms contribute little to this energy balance. The production due to coherent shear stress is everywhere positive so one does not have to add the normal stress terms in order to change its sign near $y = y_m$ as it was done in (2.4) (recall also the discussion associated with figure 13). The production of coherent eddies by the mean rate of strain (i.e. *coherent production* $= \overline{u_{ci}\,u_{cj}}\,\partial U_i/\partial x_j$) is marked by triangles in figure 25(*a*) and compared with the total turbulent production estimated from double decomposition. According to the present definition, 85% of the maximum production of the time-dependent motion is coherent because 85% of the shear stress is. Only a negligible fraction of this term could be educed from the phase-locked and ensemble-averaged data (see the curve outlined by solid, inverted triangles in figure 25*a*).

The influx of coherent energy from the mean motion (i.e. the rate of change of coherent energy or *coherent convection* $= U_j(\partial/\partial x_j)(\tfrac{1}{2}\overline{u_{ci}\,u_{ci}})$) was calculated by assuming that $\overline{w_c'^2} = 0.8\overline{u_c'^2}$ because a similar relation held throughout the flow when the simple Reynolds decomposition was used. Unless $\overline{w_c'^2}$ is grossly overestimated then the coherent convection is approximately 50% of the total provided $(y-y_m)/y_0 < 1$, and it increases to 100% of the total in the outer region (i.e. at $(y-y_m)/y_0 > 1.5$, figure 25*b*). The increase of coherent convection is consistent with the idea that all the large scales in the outer reaches of the forced wall jet are coherent (see figure 23).

The estimated diffusion of coherent energy by the coherent velocity fluctuations (i.e. the term $(\partial/\partial x_j)(\tfrac{1}{2}\overline{u_{ci}\,u_{ci}\,u_{cj}})$) is plotted in figure 25(*c*). Only four out of the six terms were actually measured. These terms were compared and found to be equal to the terms calculated by using double decomposition throughout the flow. Thus the remaining cross-product $(\partial/\partial x_j)(\tfrac{1}{2}\overline{w_c^2\,u_{cj}})$ for $j = 1, 2$ could be imported from the term calculated by doubly decomposing the equations of motion. The data shown in figure 25(*c*) suggest that the diffusion of coherent kinetic energy by random velocity fluctuations is

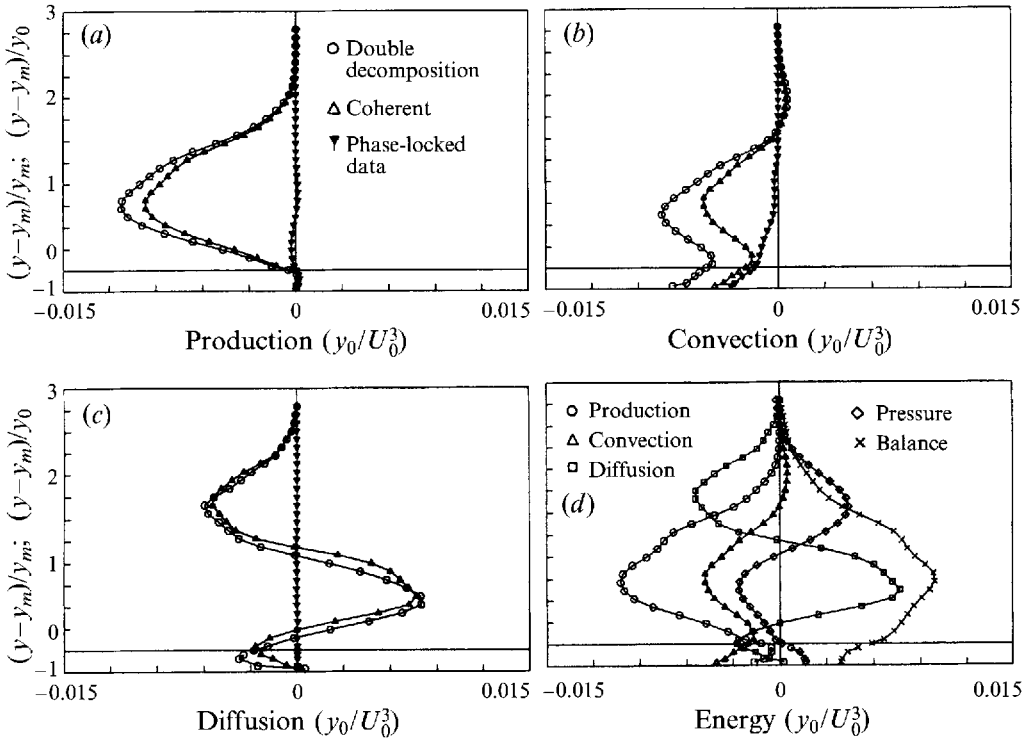

FIGURE 25. The kinetic energy budget for the large coherent eddies.

extremely small. This agrees well with independent measurement of $(\partial/\partial x_j)\overline{u_{ci}\langle u_{ri}u_{rj}\rangle}$ which is not plotted because of its insignificance.

The viscous dissipation of coherent structures $\overline{\epsilon_c}$ was estimated by using Taylor's hypothesis and found to be negligible. This result was anticipated in view of the fact that large eddies are essentially inviscid. The intermodal production terms between the random and the coherent parts of the motion (i.e. the terms $\langle u_{ri}u_{rj}\rangle \partial u_{ci}/\partial x_j$ given in (2.13)) could not have been estimated with any reasonable accuracy in this experiment since the measurements were not made with large arrays of probes and did not provide instantaneous spatial information across the wall jet. Thus terms like $(\partial u_{ci}/\partial x_j)$, or any spatial derivatives involving the correlation between coherent and random fluctuations at any given time are not really known because of the phase jitter. By equation the pressure–diffusion term for the coherent motion with the estimate made by using doubly decomposed results (shown in figure 15) one obtains the intermodal production terms from the budget itself. This is not a far-fetched assumption in view of the fact that four of the velocity diffusion terms for the coherent part of the motion turned out to be identical with the terms calculated by using double decomposition.

Coherent energy is lost to the random fluctuations throughout the flow but most of it occurs at approximately $(y-y_m)/y_0 = 0.75$ where the intensity of the coherent and incoherent eddies is strongest (figure 25*d*). The former are produced by the mean flow as a consequence of its instability while the latter are not only produced by the coherent eddies but are also diffused by them. The loss of coherent energy to random energy, resembles the dissipation term in the turbulent kinetic energy budget constructed by using double decomposition (figure 15). This could have been anticipated because most

of the energy gained and transferred by the production and diffusion terms is coherent. Since viscous dissipation in the large coherent eddies is negligible the intermodal production in the coherent budget replaces the dissipation terms when Reynolds-averaged equations are used. Small-scale eddies are created and dissipated at approximately the same locations in the flow. Consequently only the large coherent eddies extract energy from the mean flow and transport it to other locations while the random fluctuations concomitantly gain most of their energy from the coherent ones and help in dissipating it through viscosity. This is a slightly modified view of the traditional cascade process which identifies an inviscid eddy, represented by a small number of Fourier coefficients, which transfers its energy to an assortment of random small-scale dissipative eddies.

3. Conclusions

Weak excitation of a turbulent wall jet at relatively high frequencies coupling to the prevailing modes of instability existing near the surface around $x/b = 100$ had the following effects on the flow.

(i) The skin friction was reduced by approximately 7% between $x/b = 100$ and 200, in spite of the fact that the mean flow expressed by the rate of spread of the jet and by the shape of its mean velocity profile was hardly altered by the forcing.

(ii) There is a significant increase in the intensity of $\overline{u'^2}$ near the surface at $x/b < 100$ which diminished further downstream. Far away from the surface, however, the intensity of $\overline{u'^2}$ increased with x at $x/b > 100$ suggesting a transfer of energy from the surface outwards.

(iii) External excitation increased the intensity of $\overline{v'^2}$ in the outer region of the flow, but it did not affect the spanwise fluctuations $\overline{w'^2}$. Most of the increase in the intensity of the v' component occurred around the subharmonic of the forcing frequency. It had, therefore, a broader spectrum and a larger degree of jitter than was generally noticed at the forcing frequency.

(iv) The turbulent energy budget based on the conventional double decomposition of the equations of motion did not reveal the mechanism responsible for the outward transfer of turbulent energy in the wall jet. It indicated a need to decompose the equations of motion into three components consisting of a steady mean field, coherent eddies and random turbulence.

(v) A simple definition of the coherent motion allowing for phase jitter relative to the externally imposed perturbations provided an acceptable distribution of kinetic energy contained in the large eddies. More than 80% of the fluctuating 'coherent energy' is contained by three to four discrete frequencies which are equal to, or lower than, the forcing frequency. The phase-locked and ensemble-averaged procedure does not represent correctly the energy contained in the coherent structures of this flow; nevertheless, the quantitative definition proposed needs to be tested further.

(vi) The kinetic energy transferred from the large coherent eddies to the small random ones is dissipated by the latter through viscosity. Thus most of the complex interaction occurs between the mean flow and the large coherent eddies. Consequently, the energy cascade process is not just postulated but it is verified in this case.

This research was supported in part by AFOSR grant number F49620-93-1-0050 monitored by Dr J. McMichael.

REFERENCES

ALCARAZ, E. 1977 Contribution a l'etude d'un jet plan turbulent evolaunt le long d'une parios convexe a faible courbure. These d'Etat. Université Claude Bernard, Lyon, France.

BLACKWELDER, R. F. & KAPLAN, R. E. 1972 The intermittent structure of the wall region in a turbulent boundary layer. *Proc. 12th IUTAM Intl Congr. of Applied Mechanics Moscow.*

GLEZER, A., KATZ, Y. & WYGNANSKI, I. 1989 On the breakdown of a wave packet trailing a turbulent spot in a laminar boundary layer. *J. Fluid Mech.* **198**, 1.

GUITTON, D. E. & NEWMAN, B. G. 1977 Self preserving turbulent wall jets over convex surfaces. *J. Fluid Mech.* **81**, 155.

HEINE, C. 1994 The energy budget in the forced turbulent wall jet. Dipl. Ing. Thesis, Technical University, Berlin.

HESKESTADT, G. 1965 The plane turbulent jet. *Trans. ASME* E: *Appl. Mech.* **32**, 721.

HINZE, J. O. 1975 *Turbulence.* McGraw Hill.

HUSSAIN, A. K. M. F. 1983 Coherent structures – reality and myth. *Phys. Fluids* **26**, 2816.

IRWIN, H. P. A. H. 1973 Measurements in a self preserving plane wall jet in a positive pressure gradient. *J. Fluid Mech.* **61**, 33.

KARLSSON, R. I., ERICSSON, J. & PERSSON, J. 1992 LDV measurements of a plane wall jet in a large enclosure. *Internal Rep.* Department of Hydromechanics, Royal Institute of Technology, Sweden.

KATZ, Y., HOREV, E. & WYGNANSKI, I. 1992 The forced turbulent wall jet. *J. Fluid mech.* **242**, 577 (referred to herein as KHW).

KLEBANOFF, P. S. 1955 Characteristics of turbulence in a boundary layer with zero pressure gradient. *NACA Rep.* 1247.

KRUKA, V. & ESKINAZI, S. 1964 The wall jet in a moving stream. *J. Fluid Mech.* **20**, 555.

LAUFER, J. 1954 The structure of turbulence in a fully developed pipe flow. *NACA Rep.* 1174.

LAUNDER, B. E. & RODI, W. 1981 The turbulent wall jets. *Prog. Aerospace Sci.* **19**, 81.

NARASIMHA, R., NARAYAN, K. Y. & PARTHASARATHY, S. P. 1973 Parametric analysis of turbulent wall jets in still air. *Aero. J.* **77**, 355.

OSTER, D. & WYGNANSKI, I. 1982 The forced mixing layer between parallel streams. *J. Fluid Mech.* **123**, 91.

ROTTA, J. C. 1962 Turbulent boundary layer in incompressible flow. *Prog. Aero. Sci.* **2**, 1–219.

TAILLAND, A. & MATHIEU, J. 1967 Jet parietal. *J. Méc.* **6**, 103.

TENNEKES, H. & LUMLEY, J. L. 1972 *A First Course in Turbulence.* MIT Press.

WYGNANSKI, I., HARITONIDIS, J. H. & KAPLAN, R. E. 1979 On a Tollmien-Schlichting wave packet produced by a turbulent spot. *J. Fluid Mech.* **92**, 505.

WYGNANSKI, I., KATZ, Y. & HOREV, E. 1992 On the applicability of various scaling laws to the turbulent wall jet. *J. Fluid Mech.* **234**, 669.

ZHOU, M. D., HEINE, C. & WYGNANSKI, I. 1993 The forced wall jet in an external stream. *Proc. AIAA Shear Flow Conf. Orlando. AIAA Paper* 93-3250.

ZHOU, M. D. & WYGNANSKI, I. 1993 Parameters governing the turbulent wall jet in an external stream. *AIAA J.* **31**, 848 (referred to herein as ZW).